METALLOGRAPHY

This chapter presents a selection of metallographic concepts and methods essential to the understanding of basic processes in powder metallurgy – in particular iron powder metallurgy. The somewhat shorthanded presentation of some items may stimulate the reader to collect further information from pertaining special literature.

TABLE OF CONTENTS

1.1 The natural states of matter

All matter surrounding us consists of atoms, ions and molecules, which, depending on their mutual distances, are under the influence of stronger or weaker reciprocal forces. Depending on the strength of their reciprocal forces, these particles form gases, liquids or solids.

In gases. The particles (i.e. atoms, ions or molecules) move about highly irregularly at very high speeds (some 100 m s^{-1} at R.T.). Their *free length of way,* δ, (i.e. the distance a particle can move before colliding with another one) is large compared to the particle diameter. Their density is in the order of 10^{19} / cm^3. This situation is called *random order. See Fig. 1.1 a.*

In liquids. The particle density is in the order of 10^{22} / cm^3. The particles move about rather irregularly but are more crowded than in the gaseous state, each particle having approximately ten very close neighbors. Significant of liquids is the frequent local formation of crystal-like agglomerates extending over several particle diameters. Because of the high thermal energy of the particles, these agglomerates are very short-lived and there is no correlation between more distant particles. This situation is called *instable short-range order. See Fig. 1.1 b.* In contrast to gases and liquids, amorphous and crystalline materials exhibit, within a certain range of temperatures, a considerable rigidity – they are solids.

In amorphous solids. The particle density is of the same order of magnitude as in liquids, i.e. $10^{22}/cm^3$. Similar to liquids, a short-range order exists between particles. But in contrast to liquids, due to the heavily restricted mobility of the particles in amorphous solids, this order is stable and, logically, it is called *stable short-range order. See Fig. 1.1 c*. Amorphous materials have no sharply defined melting point. The transition from their solid to their liquid state occurs gradually. They can, in fact, be looked at as liquids with an extremely high viscosity at room-temperature. Classic examples are glasses. But today, by means of special processes, also metals can be transformed into an amorphous state.

In crystalline solids. Such as metals, the particle density is in the order of 10^{23} /cm^3 , i.e. ten times higher than in liquids and amorphous materials. The particles are homogeneously distributed and form a strict geometrical structure. *See Fig. 1.1 d.* Their mobility is restricted to very small vibrations about fixed equilibrium sites. These vibrations increase with temperature. This situation is called *crystalline long-range order.* The crystalline state possesses the lowest internal energy of all states of matter and, therefore, is stable below a sharply defined melting point. The above mentioned states are not specific to any particular kind of material. In principle, but not always in practice, any type of material can adopt any of these states.

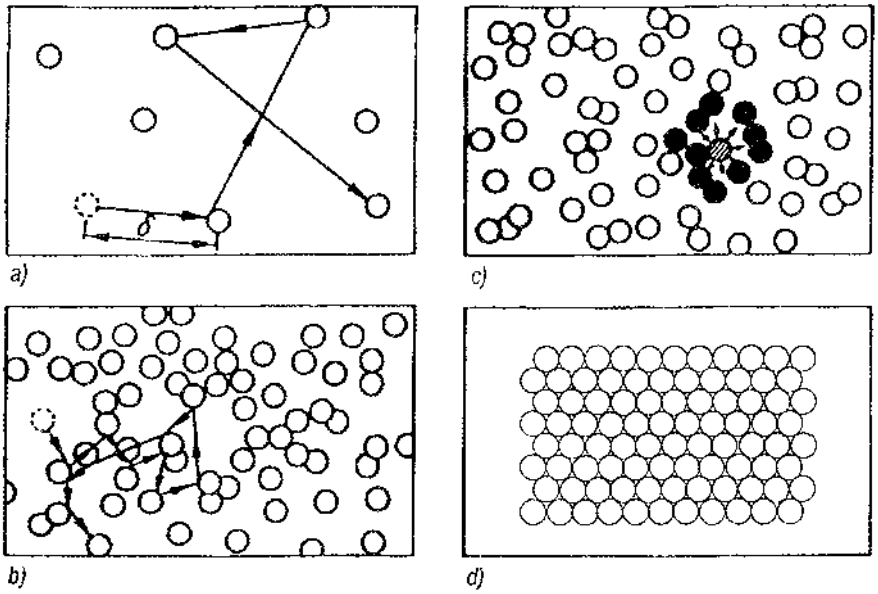

Figure 1.1 Distribution of atoms in gases, liquids, amorphous and crystalline solids (schematically);
a. Gas: *statistical distribution*, particle density = $10^{-19}/cm^3$, δ = free length of way.
b. Liquid: *instable close-range order*, particle density = $10^{-22}/cm^3$.
c. Amorphous solid: *stable close-range order*, particle density = $10^{-22}/cm^3$.
d. Crystal: *crystalline order*, particle density = $10^{-23}/cm^3$.

1.2 The crystalline structure of metals

Our further considerations are focused mainly on the crystalline – in particular the metallic – state of matter. The formation of crystalline structures is controlled by certain binding-forces between the atoms. Geometrical descriptions of crystalline structures refer to so-called *ideal crystals* only and do not take into account disturbances occurring in real crystals, such as surfaces, grain-boundaries, dislocations, vacancies, foreign atoms and other irregularities. In the following paragraph, we will discuss;
1) various types of bonding between atoms,
2) structures of ideal crystals,
3) stacking faults and disturbances in real metal crystals, and
4) plastic deformation in metal crystals.

1.2.1 Bonding between atoms

Crystal structures owe their existence to various types of interatomic forces between neighboring atoms. Four characteristic types are recognized: *van der Waals*, *covalent*, *ionic* and *metallic*.

Van der Waals force. This is the only appreciable force exerted between well separated atoms and molecules. It is a weak attractive force that acts between all atoms and is responsible e.g. for the condensation of noble gases and chemically saturated molecules to liquids and solids at low temperatures. Its explanation requires quantum mechanics because it involves fluctuations of the electronic charge in the atom.

When two atoms approach fairly closely these fluctuations can occur in unison so that one atom has its electrons slightly nearer the other nucleus whenever this nucleus happens, through the movements of its own electrons, to be more exposed in this direction than usual.

Ionic bond. Neighboring atoms exchange electrons and the so formed positive and negative ions are pulled together electrostatically as, for example, in NaCl-crystals.

Covalent bond. Partly empty electron shells of neighboring atoms overlap so that their electrons belong to both atoms. This leads to strong bonds between the atoms because in the overlapping shells their electrons are in a lower state of energy than in separate shells. One important feature of these bonds is that they can exist between atoms of the same type between which there can be no ionic bonding. Examples are H_2 ,O_2 and Cl_2. One other important feature of these bonds is that they act in preferential directions as, for example, in the tetrahedral structures of the CH_4-molecule and of diamond.

Metallic bond. This type of bond can be explained only on the basis of the following quantum-mechanical principle. All atoms in the metal crystal form one common band of electron shells to which each individual atom contributes one electron. These electrons, not being bonded to individual atoms, can move freely inside the entire metal crystal. They form a so-called *electron gas*.

According to an obsolete electrostatic theory, the negatively charged electron gas presses the negatively charged metal ions closely together. But the correct explanation is that the mentioned arrangement constitutes the lowest possible quantum state of energy for the metal crystal and allows the atoms to be packed in the closest possible way, To this kind of close packing, metals owe their good plastic formability. The freely moving electrons are responsible for the high electrical and thermal conductivity of metals and for the characteristic metallic gloss.

The overwhelming majority of all chemical elements crystallize in metal structures, approximately one third of them each in BCC-, in FCC- and in CPHex-structure.

See Table 1.1. The geometrical characteristics of these particular structures are described in the following paragraph.

Table 1.1. Crystal structures and lattice constants of some metals. [T.1.1]

Structure	Metal	Temperature C°	Lattice Constants a) 10^{-10} m; c) 10^{-10}m	Ratio of Lattice Constants c / a
BCC	α-Fe		2,286	
	δ-Fe	1390	2,932	
	Cr		2,884	
	Mo		3,147	
	W		3,165	
	β-Ti	900	3,306	
FCC	Ni		3,524	
	δ-Co	467	3,560	
	Cu		3,619	
	γ-Fe	1000	3,651	
	Ir		3,839	
	Pt		3,923	
	Al		4,049	
	Au		4,078	
	Ag		4,086	
	Pb		4,950	
CPHex	α-Co		2,506; 4,068	1,62
	Zn		2,665; 4,947	1,86
	α-Ti		2,950; 4,679	1,59
	Cd		2,979; 5,617	1,89
	Mg		3,209; 5,210	1,62
	(ideal)			1,633

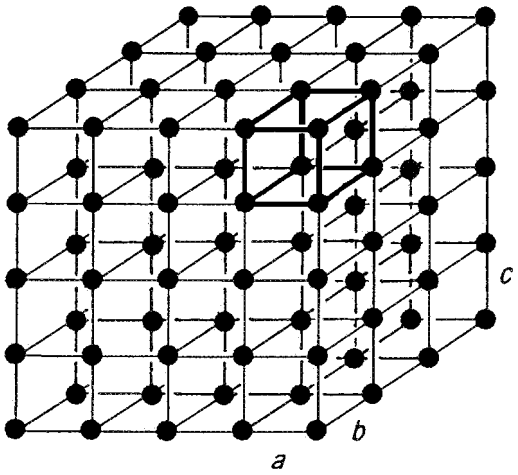

Figure. 1.2. Unit cell in a crystal cell; lattice constants: a, b, c.

1.2.2 Ideal crystals

A crystal structure has three general properties: *periodicity, directionality* and *completeness*. *Periodicity* is the regular repetition in space of the atomic unit of the crystal (wallpaper pattern). It is the basis of the remarkable plastic properties of crystals. *Directionality* of the crystal structure appears in the fact that properties like conductivity and elasticity vary with the direction of their measurement. *Completeness* is simply the filling of all crystal sites defined by the periodic structure with the required atoms.

In crystallography, it is customary to present a crystal structure graphically as a *space lattice* within which the sites of atoms are marked by points (or small circles). These points are referred to as *lattice points*. The basic unit of the crystal structure which repeats itself in all three directions of space is called *unit cell*. The defining edges of this cell are referred to as *lattice constants*, (usually a, b, c). *See Fig. 1.2.*

The lattice points lie at the intersections of three families of parallel planes, called *lattice planes*. The distance between neighboring lattice planes is usually designated by the triple-indexed symbol $d_{h\,k\,l}$. *See Fig. 1.3.*

The spatial orientation of any lattice plane is clearly defined by its so-called *Miller indices* (h k l), which are determined in the following way:

- Choose a coordinate system with the origin at the corner of one unit cell and with its axes parallel to the edges a, b, c of this unit cell.
- Determine the intersections of the plane with the tree axes, x y z, of this coordinate system.

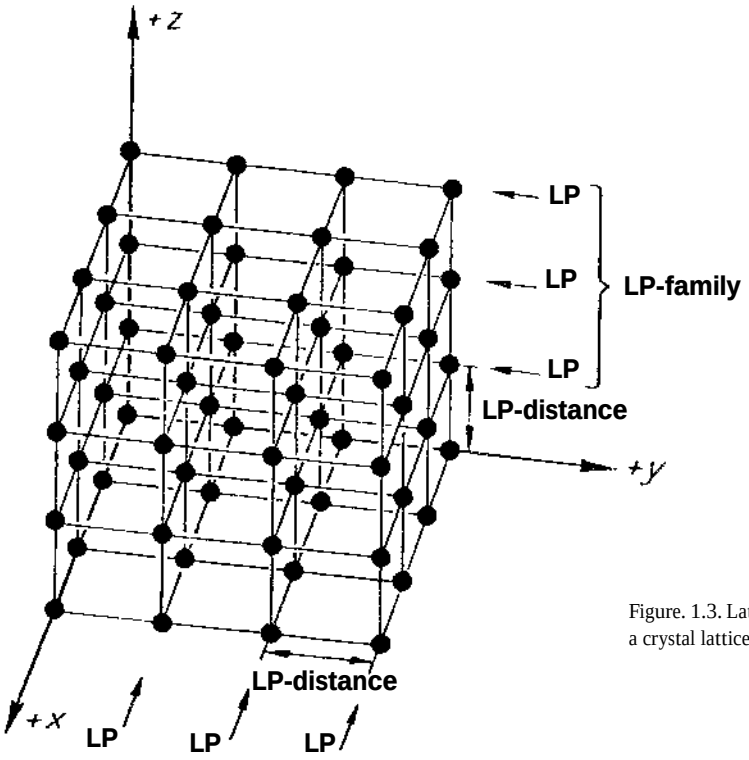

Figure. 1.3. Lattice planes (LP) in a crystal lattice.

- Express, in units of a, b, c, the distances of these intersections from the origin of the coordinate system: ma, nb, pc.
- Take the reciprocals 1/m, 1/n, 1/p and find three natural numbers related to one another in the same way as the reciprocals: 1/m : 1/n : 1/p = h : k : l. Put the result between round brackets: (h k l).
- Example: The plane, shown at *Fig. 1.4*, intersects the coordinate axes at 2a, 4b and 1c respectively. The above procedure applied to this plane yields m = 2, n = 4, p = 1. Thus, it follows: 1/2 : 1/4 : 1 = 2 : 1 : 4, and the Miller indices of this plane are: (h k l) = (214).

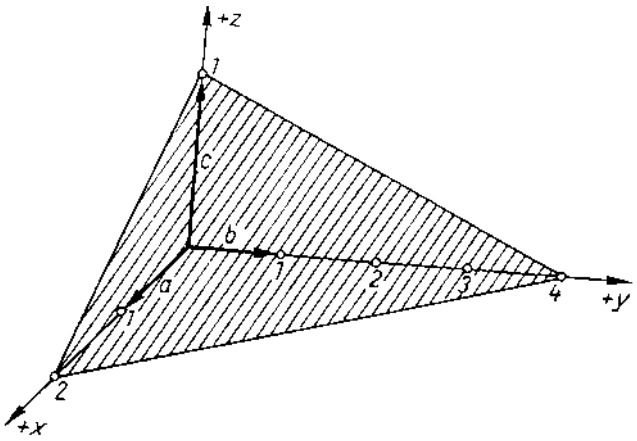

Figure. 1.4. Derivation of Miller indices.

Lattice planes and their Miller indices play an important roll e.g. in X-ray structural analysis. Each family of planes is responsible for specific X-ray reflections from which the respective Miller indices can be calculated and conclusions can be drawn as to the type of crystal structure.

Some significant lattice planes of the cubic crystal system and their respective Miller indices are shown schematically at *Fig. 1.5.*

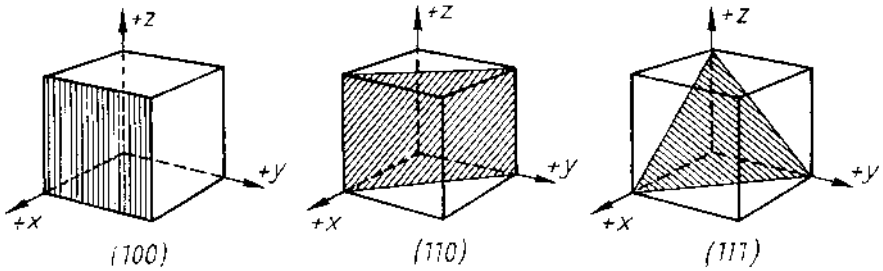

Figure. 1.5. Miller indices for some important lattice planes in cubic crystals.

Not only lattice planes but also *lattice directions* can be described by Miller indices. A lattice direction is defined as the direction of a local vector $\mathbf{r} = u\,\mathbf{a} + v\,\mathbf{b} + w\,\mathbf{c}$, originating from the corner of a unit cell, a, b, c being the edge vectors of the cell (unit vectors of the coordinate system x, y, z).

The statement of the three coordinates of the vector in square brackets [uvw] definitely identifies a given lattice direction. In the cubic system (and only there), a

lattice direction [uvw] is always perpendicular to the lattice plane (hkl) of same indices (h = u, k = v, l = w). The coordinates of the local vector r, put in double square brackets [[uvw]], specify a lattice point. Some lattice directions and lattice points are indicated in the schematic drawing at *Fig. 1.6*.

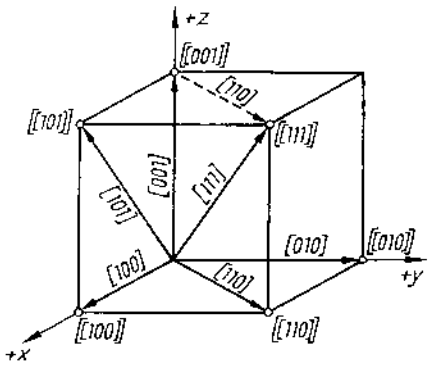

Figure. 1.6. Lattice points and lattice directions in the cubic crystal system.

For the characterization of lattice planes, directions and points in hexagonal crystal systems, four instead of three Miller indices are required. Their detailed description can be found in pertaining special literature and has no bearing on our further discussions.

As already mentioned, all metals crystallize either in a body-centered-cubic (BCC), in a face-centered-cubic (FCC) or in a close-packed hexagonal (CPHex) structure. The respective unit cells of these structures are shown at *Fig. 1.7*.

The dice-shaped unit cells of the BCC- and of the FCC-structure are each presented in two different ways: to the left as abstract point lattice, and to the right as conglomerate of spheres. The sphere-model conveys a fairly realistic picture of the packing structure of the atoms inside the crystal.

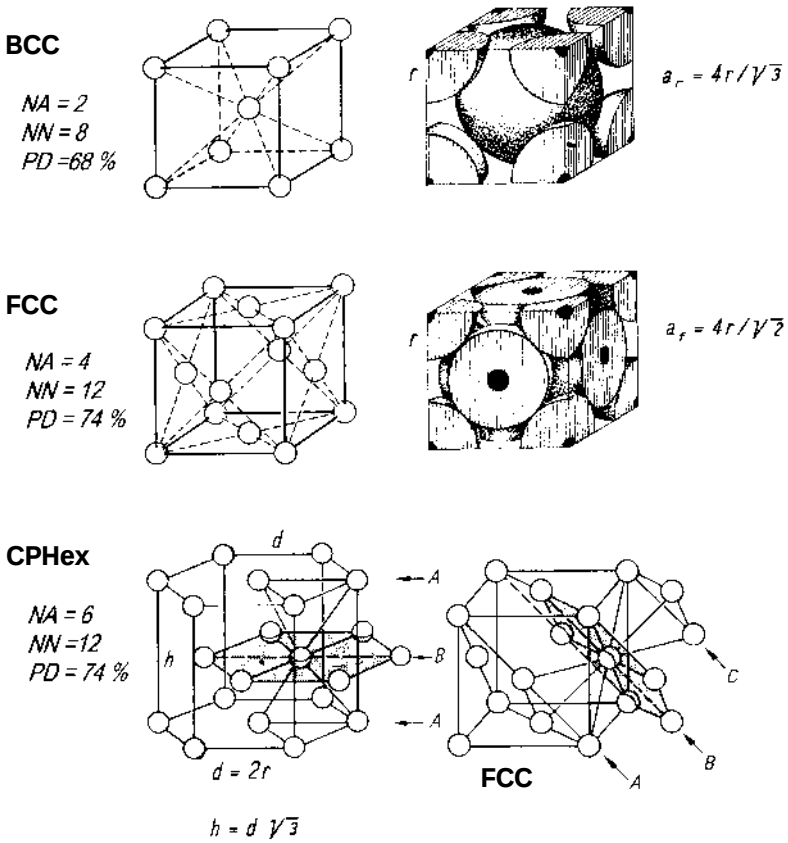

Figure. 1.7. Unit cells of some important crystal structures: body-centered cubic (BCC); face centered cubic (FCC); and close-packed hexagonal (CPHex). NA = number of atoms/elementary cell; NN = number of nearest neighbors; PD = packing density.

From the unit cells presented at *Fig. 1.7*, three significant parameters can be derived, viz. the number of atoms per unit cell, *NA*, the number of nearest neighbors, *NN*, and the packing density *PD*. The number of atoms, *NA*, is easily obtained in the following way:

- In the case of the BCC-cell, putting together to 1 whole atom the 8 eighth of an atom from each corner of the cell, and adding the one whole atom from the center yields 2 whole atoms per unit cell: *NA* = 2.

- In the case of the FCC-cell, putting together to 1 whole atom the 8 eighth of an atom from each corner of the cell, and putting together to 3 whole atoms the 6 halves of an atom from the faces of the cell, yields 4 whole atoms per cell: *NA* = 4.
- In the case of the CPHex-cell, putting together to 2 whole atoms the 12 sixth of an atom from the corners of the cell, putting together to 1 whole atom the two halves of one atom from the hexagonal faces, and adding the three atoms from inside the cell yields 6 atoms per cell: *NA* = 6.

Obviously, for the BCC-cell, the number of nearest neighbors is *NN* = 8. The number of nearest neighbors for the FCC- and for the CPHex-cell becomes evident when looking at the plane of close-packed atoms (shaded), within which each atom has 6 nearest neighbors. In addition, each atom has 3 nearest neighbors each in the two planes above and beneath the shaded plane. All together, they add up to 12 atoms: *NN* = 12.

Both, in the FCC- and in the CPHex-structure, atoms are packed at maximal possible density, viz. PD ≅ 74 %. The packing density of the atoms in the BCC-structure is only PD ≅ 68 %. The reader can easily verify these two figures by dividing the volume of atoms belonging to one unit cell ($NA \bullet 4\pi\, r^3/3$) with the volume of this cell (a^3).

At *Fig. 1.7*, for comparison, fully close-packed lattice planes in the CPHex- and in the FCC-structure are marked by shading. The diagram at *Fig. 1.8* (a) shows a fully close-packed plane. The spheres or atoms lie in three sets of close-packed lines, physically equivalent and symmetrically orientated to one another. Both, the CPHex- and the FCC-crystal structure are formed by stacking a number of close-packed planes on one another in a certain *stacking sequence*.

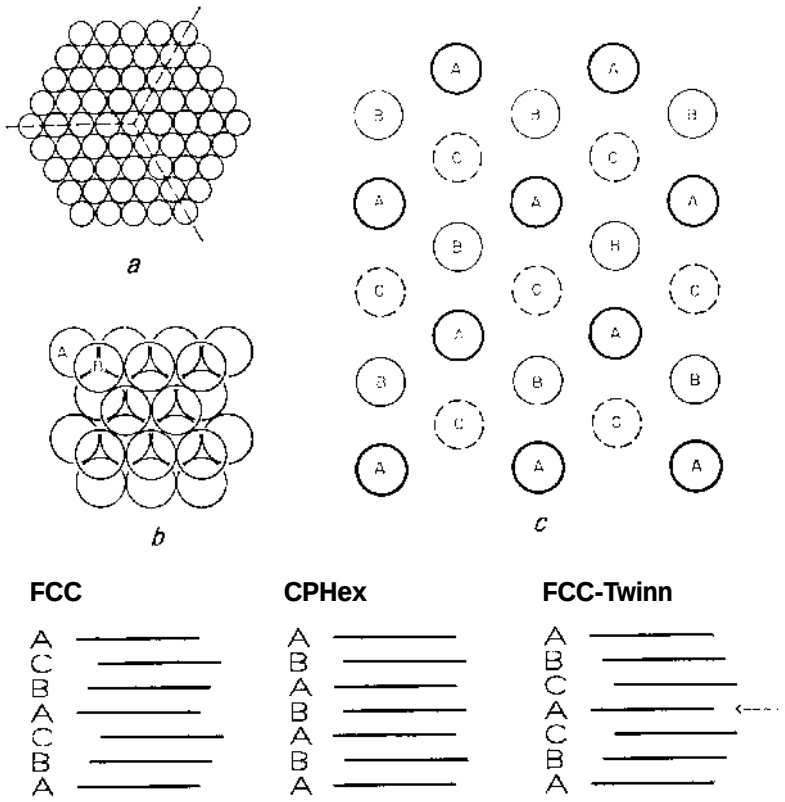

Figure. 1.8. Arrangement of atoms in a close-packed plane (a), and in successive close-packed planes (b) and (c). Below: stacking sequences of close-packed planes in FCC and CPHex crystals.

The diagram at *Fig. 1.8 (b)* shows an element of the stacking sequence, a layer B laid on a similar layer A in the most closely packed way. The layers have the same orientation and each B atom rests symmetrically in a hollow provided by three adjoining A atoms. We notice that only one-half of the hollows are used by B atoms and that an equally close-packed arrangement would result if we had used the other hollows, i.e. the C positions in diagram (c), instead.

Any stacking sequence chosen from the A, B and C positions is fully close-packed provided positions of the same type are not used by neighboring planes. For example, ABACBABAC is close-packed but ABBAAACCBBC is not.

The stacking sequence ABABAB… forms the CPHex-structure, and ABCABCABC… forms the FCC-structure. In FCC-structures, the stacking sequence occasionally forms mirror images of itself like ABC(A)CBA(C)ABC.

This kind of stacking faults is called *twinning*. Crystal twins occur frequently in copper, nickel and austenitic steels and appear on micrographs as parallel stripes inside the crystal grains.

1.2.3 Real Metal Crystals

All metals used in technical applications (apart from single crystals and whiskers) have a *polycrystalline* structure, i.e. they are composed of many randomly oriented small crystal grains agglomerated to one another. When cooling down a molten metal below its melting point, at first, very small dendrites (crystal nuclei) precipitate from the melt. These dendrites gradually develop into small crystallites which randomly oriented float around in the melt. Independently of one another, the floating crystallites continue to grow, gradually depriving the melt of atoms. Eventually, they get so crowded in the diminishing melt that they begin to agglomerate. *See Fig. 1.9.*

Because of their original random orientation, a misfit between crystal lattices occurs at the boundaries of adjoining crystallites (or crystal grains). In these grain boundaries, atoms are not quite so closely packed as in the undisturbed lattice inside the crystal grains. On a polished and etched metallographic section, grain boundaries usually appear as thin dark lines.

Apart from grain boundaries, there are several other kinds of lattice disturbances in real crystals. One distinguishes between zero-, one-, two-, and three-dimensional lattice disturbances.

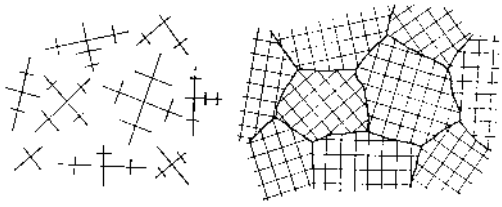

Figure. 1.9. Formation of a polycrystalline structure during solidification of a liquid metal (schematically);
left: nucleation period (dendrites floating in the melt);
right: end of solidification (agglomerated crystallites).

Zero-dimensional lattice disturbances are
1) missing atoms in the regular lattice structure, (so-called *vacancies*),
2) foreign atoms occupying interstices between host atoms (*interstitial atoms*, and
3) larger or
4) smaller foreign atoms substituting atoms of the host lattice (*substitutional atoms*).
See Fig. 1.10.

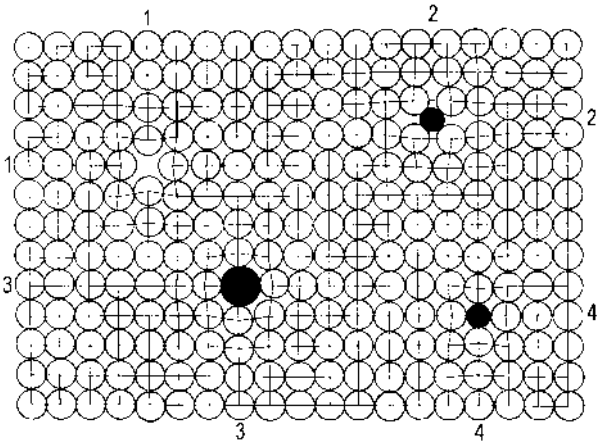

Figure. 1.10. Zero-dimensional lattice disturbances:
(1-1) vacancy,
(2-2) interstitial atom,
(3-3) and,
(4-4) bigger and smaller substitutional atoms.

One-dimensional lattice disturbances are so-called *dislocations* which occur in two different varieties, *edge dislocations* and *screw dislocations*, forming zones of lower packing-density which like filaments stretch through the crystal structure. The schematic drawings at *Fig. 1.11* shows one edge dislocation (a) and one screw dislocation (b).

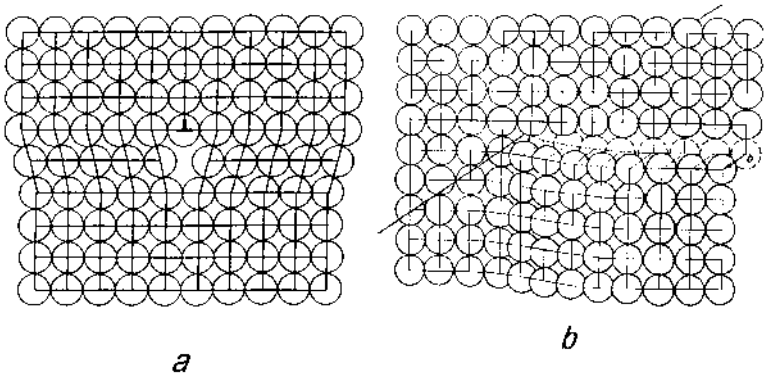

Figure. 1.11. One-dimensional lattice disturbance: (a) edge dislocation, (b) screw dislocation; in both cases, the dislocation line is perpendicular to the drawing plane.

Two-dimensional lattice disturbances are the above mentioned grain boundaries, which can also be imagined as arrays of edge dislocations stacked on top of one another. *See Fig. 1.12*.

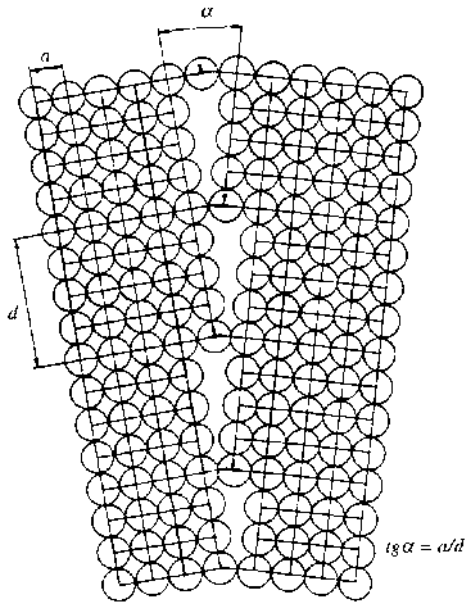

Figure. 1.12. Two-dimensional lattice disturbance: a grain boundary (composed of an array of dislocation lines stacked on top of each other) the grain boundary face is perpendicular to the drawing plane.

Three-dimensional lattice disturbances are non-metallic inclusions, dislocation tangles, and small pores as occur in certain diffusion processes (Kirkendall-effect) and in sintering processes.

1.2.4 Plastic Deformation of Metal Crystals

Dislocations play the most essential part in plastic deformation of metals. Under the influence of shearing-stresses, dislocations are created, and slip occurs on certain lattice planes (mainly (111)-planes). On these slip planes, dislocation lines move like waves along energetically favorable directions (mainly [111]-directions).

This kind of slipping is facilitated by the circumstance that bonds between adjacent atoms on both sides of the slip plane are not been broken all at the same time but successively one after the other. *See Fig. 1.13*.

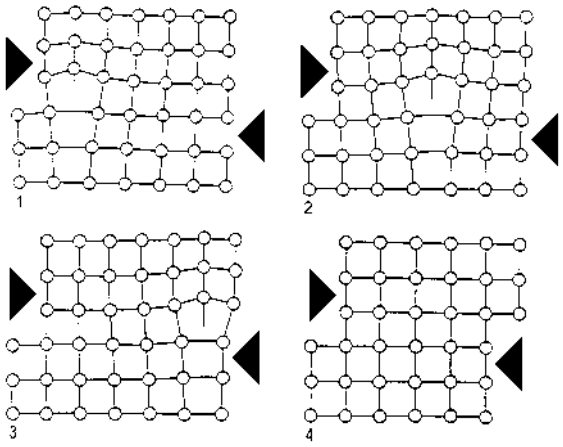

Figure. 1.13. Atomic bonds transiently being ruptured as dislocation travels through crystal under the influence of shearing stresses.

Along a dislocation line perpendicular to the direction of slip, bonds are temporarily suspended. As shown schematically at *Fig. 1.14*, the dislocation line, driven by shearing-stresses, travels through the crystal achieving a small displacement of the upper half of the crystal against its lower half.

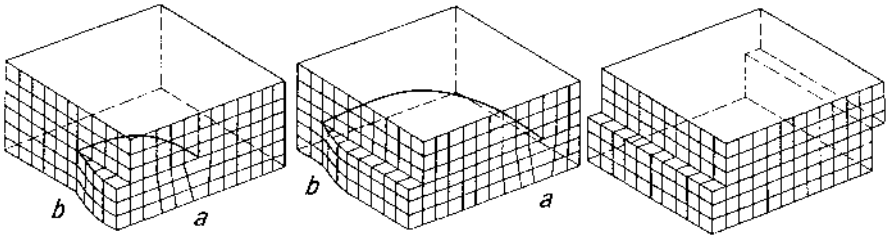

Figure. 1.14. Dislocation line, stretching from edge dislocation (a) to screw dislocation (b), travels through a crystal, shifting its upper half relative to its lower half by atomic distance.

In order to achieve a noticeable plastic deformation, a great many dislocation lines must travel through the metal. The more crowded the dislocations get, the more do they interfere with one another: They get entangled, pile up against grain boundaries (ends of slip planes) and catch on with inclusions and other lattice disturbances. *See Fig. 1.15.*

The jamming and entangling dislocations build up a growing resistance against further deformation which eventually ceases, unless shearing-stresses are increased. This is the cause of the phenomenon of deformation hardening and a contributing cause to dispersion hardening and other hardening processes.

When the temperature is raised, dislocations gradually dissemble as atoms escape from them via vacancies. This dissembling mechanism is called *dislocation climbing*.

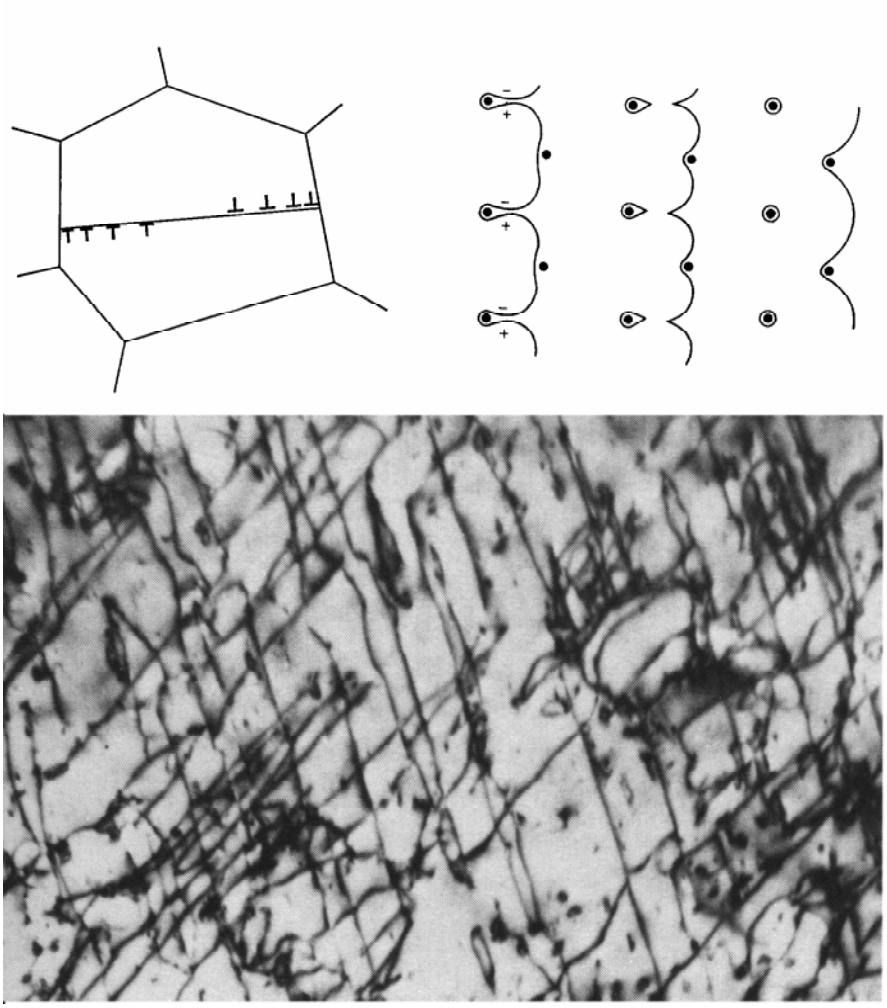

Figure. 1.15. Obstacles hampering the movement of dislocations; Top left: dislocations pile up against grain boundaries (schematically); Top right: dislocation lines traveling from left to right catch on with inclusions (schematically); Bottom: single dislocations (black lines) and dislocation tangles (diffuse black spots) in a-iron with 0.91 at.-% Cu, plastically deformed by 4 %, 50 000:1 replica. [1.1]

See Fig. 1.16. Dissembling of jammed and entangled dislocations is the mechanism behind the effect which soft-annealing has on cold-deformed metals. The fact that metals deform easier at elevated temperatures is due the following two processes:

1) the increased number and greater mobility of vacancies in the metal facilitate the dissembling of dislocations, and

2) the thermal vibration of the atoms in their lattice sites is intensified. Both processes have a lowering effect on the metals resistance to deformation, i.e.on its yield point.

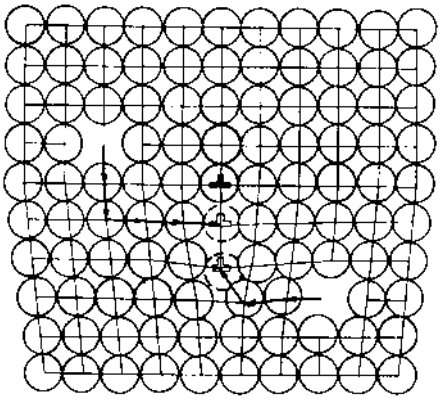

Figure. 1.16. Dislocation climbing:
A dislocation dissembles gradually as atoms escape from it via vacancies.

1.3 Diffusion in Metals

All processes and reactions taking place in gases, liquids or solids are depending on the thermally activated exchanges of atomic particles controlled by laws of thermodynamics and statistics. In homogeneous materials, the thermally activated particles move around in all directions without any preference. When gradients of temperature, pressure, concentration or electrical potential occur in the material, the irregular movement of particles is superimposed by a drift in the direction of the gradient (similar to a mosquito swarm drifting in the wind). This drift of atomic particles is called (directional) *diffusion*. Diffusion usually accomplishes a noticeable transport of material as, for instance, in the formation or transformation of alloys and in the sintering of metal powders.

The movement and exchange of atoms in solid metals is feasible in various ways. Inside the crystal lattice of the metal, small foreign atoms can move relatively easily from interstice to interstice between the host atoms. This kind of atom movement is called *interstitial diffusion*. *See Fig. 1.17 (a)*.

The host atoms themselves and substitutional atoms can move only from one vacancy to another. This kind of atom movement is called vacancy diffusion or, pertaining to the host atoms, *self-diffusion*. *See Fig. 1.17 (b)*. More easily than in the close-packed lattice structure, atoms can diffuse along the less closely packed grain boundaries and most easily along surfaces. Accordingly one speaks of *volume-diffusion*, *grain-boundary-diffusion* and *surface-diffusion*.

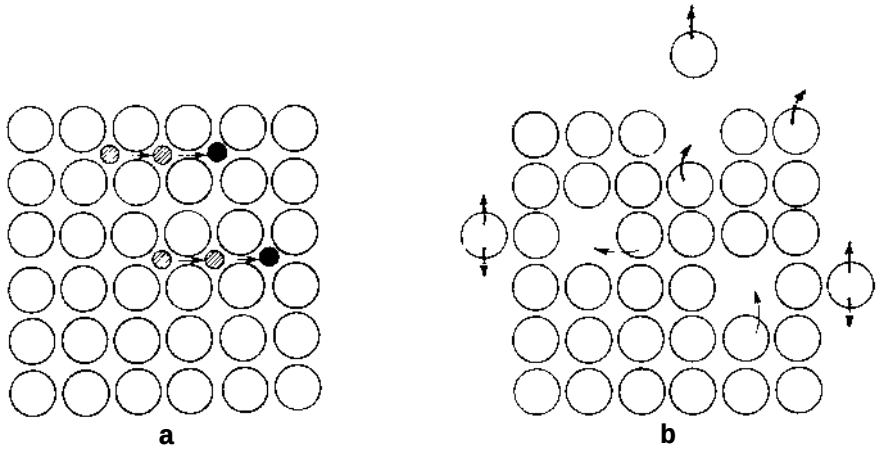

Figure. 1.17. Interstitial diffusion (a) and vacancy diffusion (b); (schematically).

1.3.1 Laws of Diffusion

In heterogeneous materials, concentration differences tend to level, because an even distribution of concentration constitutes a state of minimal free enthalpy. According to Fick's first law of diffusion, the number *d*n of atoms passing through an area A perpendicular to the direction of their movement, during a short time interval *d*t, is proportional to the concentration gradient -*d*c/*d*x residing at the location of area A:

$$\frac{1}{A}\cdot\frac{d\,n}{d\,t} = -D\cdot\frac{d\,c}{d\,x} \qquad (1.1)$$

The proportionality factor D is called *diffusion coefficient* and is usually measured in $cm^2\ s^{-1}$. Equation (1.1) applies only if the concentration gradient -*d*c/*d*x does not change during the whole diffusion process (*stationary case*). Such is approximately the case, for instance, when carbon from a hot carbonaceous gas diffuses through the thin steel wall of a furnace muffle. On its inside, the muffle is being carburized by the carbonaceous gas, on its outside decarburized by the surrounding air. As a consequence, a constant gradient of carbon concentration establishes itself in the wall, and carbon diffuses through the muffle wall at constant rate.

If, in the course of diffusion, concentration changes everywhere in the material (*non-stationary case*), Fick's second law of diffusion applies:

$$\frac{\partial c}{\partial t} = \frac{\partial}{\partial x}\left(D\,\frac{\partial c}{\partial x}\right) \qquad (1.2)$$

In cases where the diffusion coefficient D can be considered being independent of the concentration c, this equation is simplified to:

$$\frac{\partial c}{\partial t} = D\,\frac{\partial^2 c}{\partial x^2} \qquad (1.3)$$

Given the concentration distribution at the beginning of the diffusion process, this partial differential equation can be solved by means of *Gauß*' error function *erf* ( ).
A relatively simple particular solution, applicable to many practical cases, is presented in the following paragraph.

1.3.2 A Particular Solution of the Diffusion Equation

In many technical applications, the surfaces of two different metals are in such intimate contact with one another that they can exchange atoms. Such is the case e.g. when iron surfaces are protected with thin layers of zinc, copper, nickel or chromium, or in powder metallurgy where powder particles of different metallic identity are intimately pressed together in a compacting process.

In order not to confuse the understanding with complicated geometrical parameters, we choose a solution of equation (1.3) applying to the simple geometrical arrangement shown at *Fig. 1.18*: The end-faces of two oblong metal bars, A and B, are closely pressed together. This simple model illustrates the gradual leveling of concentration between two different metals which is significant of all diffusion processes. The concentration distribution at the beginning of the diffusion process is extreme, viz. 100 % A-atoms in the left bar and 100 % B-atoms in the right bar. For this model, the particular solution of equation (1.3) is:

$$c(x,t) = \frac{1}{2}\left(1 - erf\left(x / 2\sqrt{Dt}\right)\right) \qquad (1.4)$$

where c (x ,t) is the concentration of A-atoms in B at time t and distance x from the contact surface between A and B. A large variety of numerical values of Gauß' error-function erf ( ) can be found in relevant tables of mathematical textbooks.

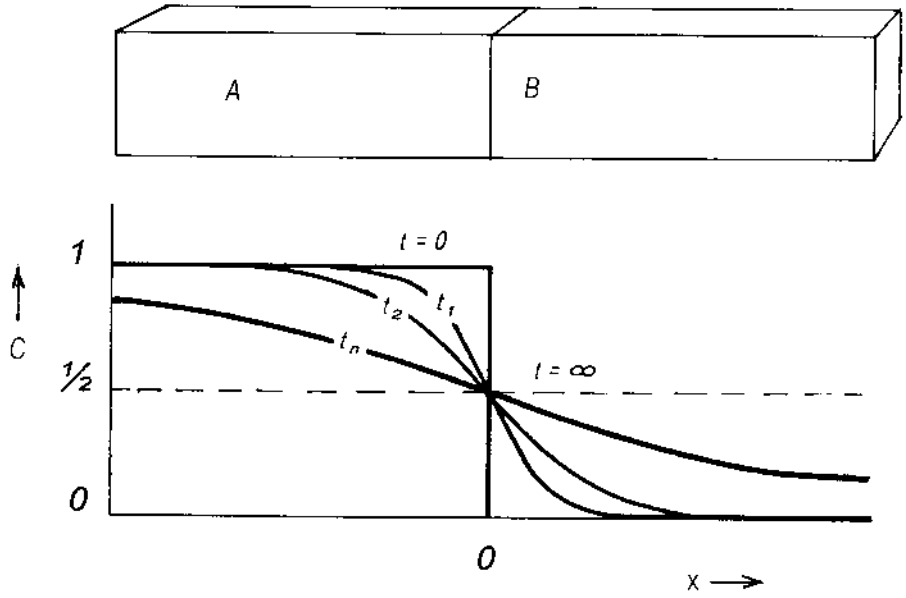

Figure. 1.18. Course of diffusion between two bars of metals A and B (schematically). Assumed are initial concentrations of 100 % A-atoms in the left and 100 % B-atoms in the right bar. The curves are drawn according to equ. (1.4) and represent the distribution of A-atoms across the two bars after different periods of time.

Remarkable with equation (1.4) is the circumstance that the concentration c (x ,t) does not depend explicitly of the individual parameters x and t but on their combination as in the expression $\mathbf{x / 2\sqrt{D t}}$. This means that any given concentration of A-atoms in B moves in x-direction (i.e. from A to B) according to the time law: $\mathbf{x \propto \sqrt{D t}}$. This time law is significant of all diffusion processes and controls e.g. the speed of growth of oxide layers on metal surfaces and the traveling speed of a carburized zone from the surface to the center of a work piece of steel.

1.3.3 The Diffusion Coefficient

The diffusion coefficient D is a measure of the *diffusion rate*. D depends of the mechanism of atom movement inside the metal and particularly strongly of temperature according to the following relationship:

$$\mathbf{D = D_0\, exp(-Q / RT)} \qquad (1.5)$$

D_0 is a characteristic property of the metal, R is the universal gas constant, T is the absolute temperature, and Q is the activation energy.

D_0 depends of the atomic weight of the diffusing atoms and of the melting temperature of the metal in which diffusion takes place. In the case of vacancy-diffusion, the activation energy is the sum of formation energy and migration energy of vacancies. In the case of interstitial-diffusion, the activation energy is identical with the traveling energy of interstitial atoms. The respective traveling energies of atoms are lower in grain boundaries and lowest on surfaces.

Plotting the logarithm of D from equation (1.5) over 1/T , one obtains a straight line with the slope Q/R. *See Fig. 1.19*. Thus, from the slope of this straight line, the activation energy of the diffusion process can easily be calculated. Deviations from the straight line indicate that several kinds of atomic movements with varying activation energies are involved in the diffusion process.

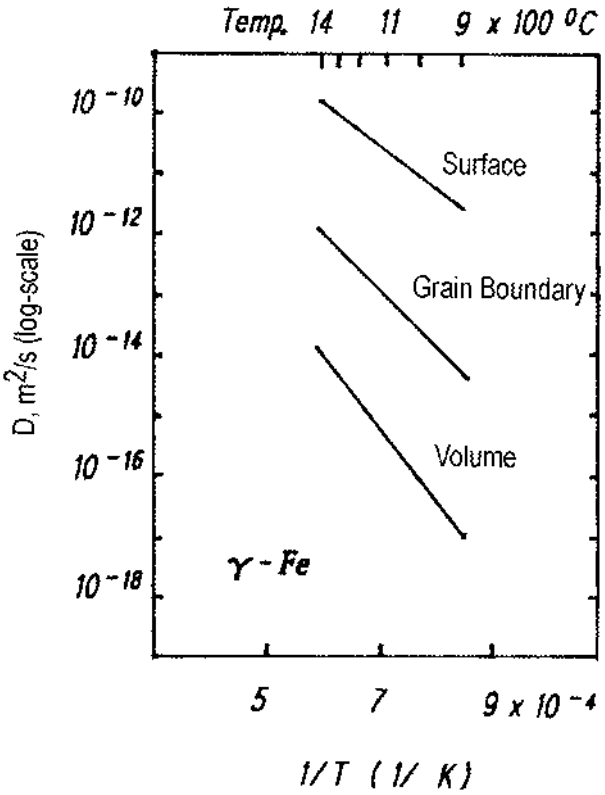

Figure. 1.19. Temperature dependence of the coefficients of self-diffusion of iron, for diffusion along surfaces and grain boundaries and inside the crystal volume (In D over 1/T).

Diffusion coefficients D, material constants D_0 and activation energies Q for some important diffusion systems are presented in Table 1.2.

Table 1.2. Physical data on some important diffusion systems

Diff. Atom	Host-Crystal	D_0 (m^2/s)	Activation Energy Q KJ/mol	kcal/mol	T (°C)	D (m^2/s)
Fe	α-Fe (BCC)	$2,0 \times 10^{-4}$	241	57,5	500 900	$1,1 \times 10^{-20}$ $3,9 \times 10^{-15}$
Fe	γ-Fe (FCC)	$5,0 \times 10^{-5}$	284	67,9	900 1100	$1,1 \times 10^{-17}$ $7,8 \times 10^{-16}$
C	α-Fe	$6,2 \times 10^{-7}$	80	19,2	500 900	$2,3 \times 10^{-12}$ $1,6 \times 10^{-10}$
C	γ-Fe	$1,0 \times 10^{-5}$	136	32,4	900 1100	$9,2 \times 10^{-12}$ $7,0 \times 10^{-11}$
Cu	Cu	$7,8 \times 10^{-5}$	211	50,4	500	$4,4 \times 10^{-19}$
Zn	Cu	$3,4 \times 10^{-5}$	191	45,6	500	$4,3 \times 10^{-18}$
Al	Al	$1,7 \times 10^{-4}$	142	34,0	500	$4,1 \times 10^{-14}$
Cu	Al	$6,5 \times 10^{-5}$	135	32,3	500	$4,8 \times 10^{-14}$
Mg	Al	$1,2 \times 10^{-4}$	131	31,2	500	$1,8 \times 10^{-13}$
Cu	Ni	$2,7 \times 10^{-5}$	255	61,0	500	$1,5 \times 10^{-22}$

1.4 Binary Phase Diagrams of Metals

1.4.1 Thermodynamics

First of all, some definitions are required:

- A *thermodynamic* state is given through the following four *parameters of state*: P, V, T and c (pressure, volume, temperature and concentration).
- A *heterogeneous system* consists of several *phases* separated by interfaces and having different properties (e.g. ice-crystals or droplets of oil in Water).
- A *phase* is in itself homogeneous and can consist of several *components* present in varying concentrations (e.g. salt water consist of H-atoms. O-atoms, Na-atoms and Cl-atoms).

Above-mentioned parameters of state given, number, type and relative amount of different phases present in a heterogeneous system are stable, when the system is in *thermodynamic equilibrium*. What is meant by this statement, will emerge from the following consideration. A system's (e.g. a metal's) internal energy E is the sum of all individual kinetic and potential energies of its particles (metal atoms). The external energy PV imposed on the system is the product of the system's volume V and the external pressure P. The sum of these two energies E + PV can also be split up according to a different aspect, namely into one part which constitutes irreversible thermal energy TS (S = entropy) and another part G which is available to accomplish work (e.g. transformation work). G is called *Gibbs' free energy* or *free enthalpy.* This interrelationship is expressed by the following equation:

$$\mathbf{E + PV = TS + G} \tag{1.6}$$

Thus, the free enthalpy (Gibbs' free energy) is given by the expression:

$$\mathbf{G = E - TS + PV} \tag{1.7}$$

The expression:

$$\mathbf{F = E - TS} \tag{1.7a}$$

is called (*Helmholtz'*) *free energy.* The differential of (1.7), constitutes the change *d*G of free enthalpy:

$$\boldsymbol{d}\,\mathbf{G} = \boldsymbol{d}\,(\mathbf{E - ST + PV}) = \boldsymbol{d}\,\mathbf{F} + \boldsymbol{d}\,(\mathbf{PV}) \tag{1.8}$$

From the *First* and *Second Law of Thermodynamics*, in case T = constant and P = constant:

$$dG = d(E - ST + PV) \leq 0 \tag{1.9}$$

and, in case T = constant and V = constant, it follows:

$$dF = d(E - TS) \leq 0 \tag{1.9a}$$

Since equilibrium reactions between metal phases usually take place at constant pressure and constant temperature but sometimes are accompanied by volume changes, equation (1.9) applies. This means that between phases striving for equilibrium, only such reactions can take place that do not increase the free enthalpy G. All reactions cease when the phases are in equilibrium and the free enthalpy G has reached a minimum[1]. The schematic diagram at *Fig. 1.20* illustrates this situation.

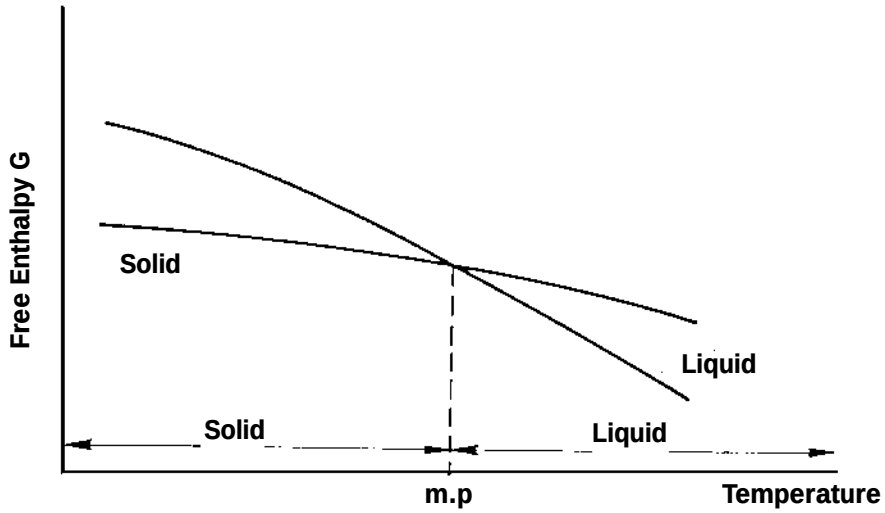

Figure. 1.20. Change of free enthalpy with temperature for a pure metal.

The free enthalpies of the liquid and of the solid state of a pure metal are plotted as functions of temperature. The two respective curves cross at the metal's melting point. Below the melting point, the free enthalpy of the solid state is lower than the one of the liquid state. Above the melting point, the relation between the two enthalpies is reversed.

1.4.2 Derivation of Binary Phase Diagrams

Applying the thermodynamic rules discussed in the preceding paragraph to a heterogeneous system involving two components A and B and two phases 1 and 2, equilibrium, at given temperature and pressure, can be achieved only by changing the concentrations of A and B in the two phases. The component A will diffuse from phase 1 to phase 2, or vice versa, until the changes of free enthalpy with changing concentration are equal with respect to both phases, viz.:

$$\frac{d G_1}{d c} = \frac{d G_2}{d c} \qquad (1.10)$$

The implication of this equation is that the two functions $G_1(c)$ and $G_2(c)$, plotted in a G-c-diagram, have a common tangent when they are in equilibrium. On the basis of these considerations, any binary diagram can be derived theoretically as long as the respective free enthalpies are known as functions of the concentration. These functions can be deduced from the *entropy of mixing* of the involved components. A discussion of entropy of mixing would exceed the frame of this chapter, and is not required for the understanding of succeeding paragraphs.

Systems with Complete Miscibility in the Solid and in the Liquid State.
For a metal system as defined in the heading to this paragraph, the free enthalpies $G_L(c)$ and $G_S(c)$ of the liquid and of the solid phase are plotted, as functions of concentration and temperature, in a schematic diagram as shown at *Fig. 1.21*. The melting point of the components A and B are denoted T_{MA} and T_{MB} ($> T_{MA}$) respectively. In the diagram, we distinguish between the following temperature ranges:

a) $T > T_{MB}$
Over the entire range of concentration, the free enthalpy curve $G_L(c)$ of the melt lies below the free enthalpy curve $G_S(c)$ of the solid. Over the entire range of concentration, only the liquid phase is thermodynamically stable.

b) $T = T_{MB}$
For c = 1 (100 %B), the free enthalpy of the melt and the free enthalpy of the solid are equal: $G_L(c) = G_S(c)$.

c) $T_{MA} < T < T_{MB}$
In this temperature range, the two free enthalpy curves cross, and each curve exhibits a minimum. The equilibrium of the two phases lies on the common tangent of the two curves in accordance with equation (1.10). The abscissas of the tangent points c_L and c_S correspond to the concentration of B in the melt and in the solid phase respectively that are in thermodynamic equilibrium.

d) $T < T_{MA}$
In this temperature range, over the whole range of concentrations, the free enthalpy curve of the solid lies below the free enthalpy curve of the melt, viz. in this temperature range, only the solid phase (composed of A- and B-atoms) is thermodynamically stable.

Thus, the ranges of thermodynamic stability of the various phases in the binary T-c-diagram (phase diagram) are separated by two theoretically deduced phase borderlines (*Liquidus* and *Solidus*).

[1] In some text books of metallography, the term free energy is used instead of the term *free enthalpy.* This does not imply a mix-up of thermodynamic functions but simply a deviation from standard terminology. What is meant, in those books, by *free energy* is, of course, *Gibbs' free energy,* i.e. *free enthalpy.*

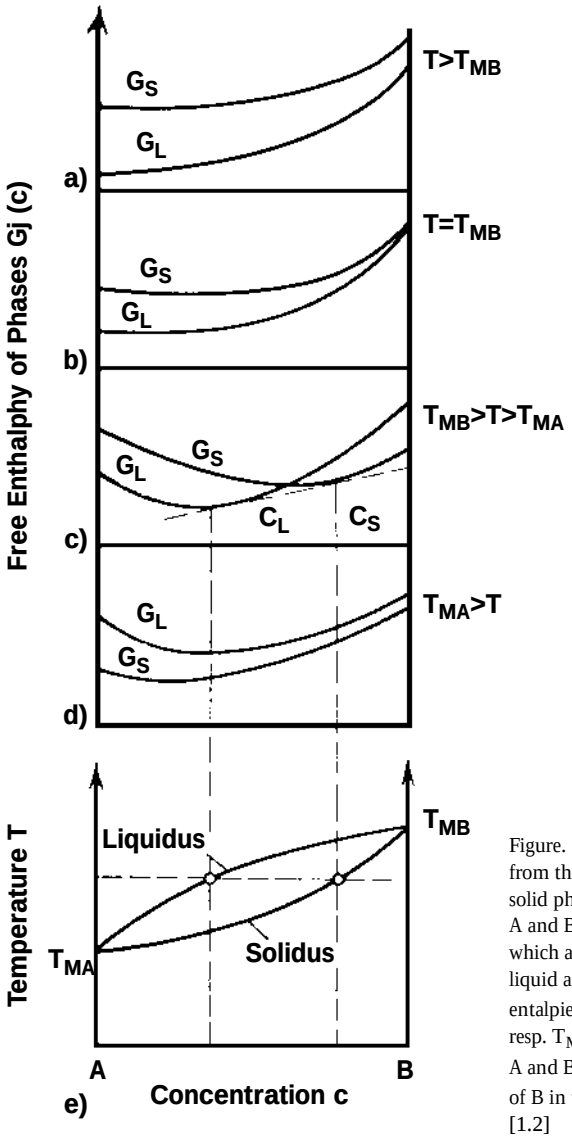

Figure. 1.21. Deriving a binary phase diagram from the free entalpy curves for the liquid and solid phases at different temperatures.
A and B are the components of the system which are completely miscible both in the liquid and solid state. G_L and G_S are the free entalpies of the liquid and of the solid state resp. T_{MA} and T_{MB} are the melting points of A and B resp. c_L and c_S are the concentrations of B in the liquid and in the solid state resp. [1.2]

Experimentally, binary diagrams can be established by means of thermal analysis. To this effect, from the two components of the system to be investigated, a number of alloys of different composition are smelted and subsequently cooled. By means of a thermocouple, the temperature changes during cooling are registered. On the so-obtained curves, phase transformations show up in the form of kinks.

These kinks are caused by thermal energy being released during phase transformation (lowering of free enthalpy) and slowing down the rate of cooling. The principle of this procedure is illustrated at *Fig. 1.22*. Typical representatives of this simple binary systemare the following pairs of metals: Cu-Ni, Ag-Au and Ag-Pd.

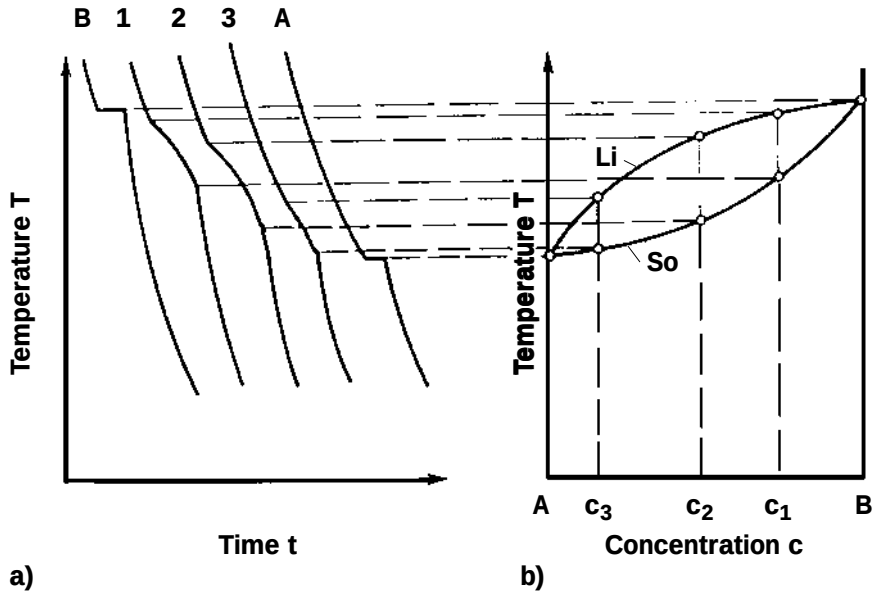

Figure. 1.22. Experimental derivation of a phase diagram by means of thermal analysis, Left: cooling curves for the two pure metals and for three of their alloys. Right: phase diagram derived from cooling curves. [1.3]

Eutectic Systems.

More complicated phase diagrams can be derived theoretically and established experimentally by methods analogous to the ones described above. As an example, we will study the binary T-c-diagram of a so-called *eutectic* system as presented at *Fig. 1.23*.

In this system, two components (metals) A and B are completely miscible in the liquid state but only to a limited degree in the solid state.

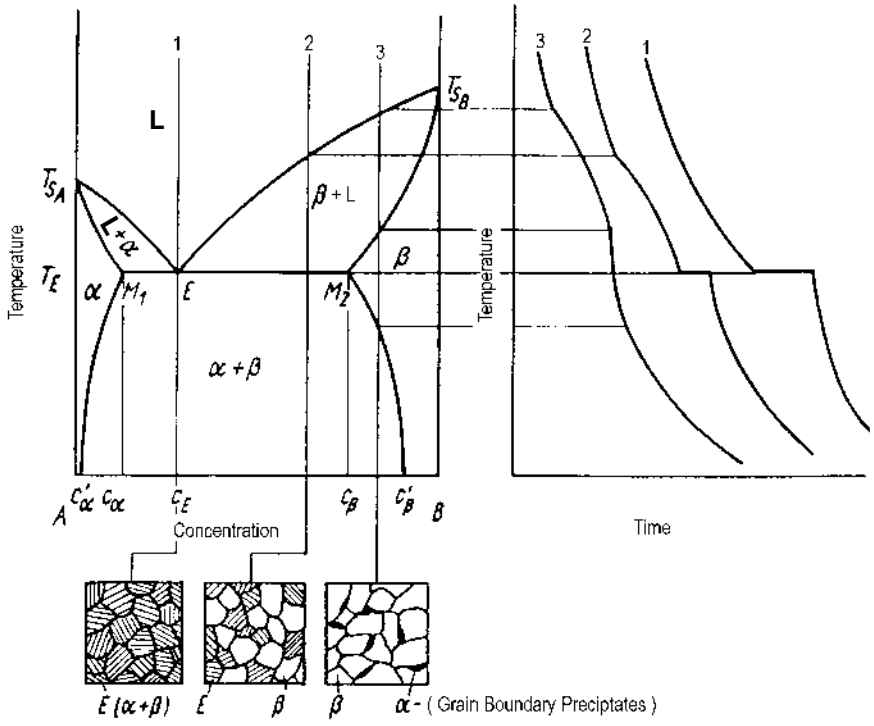

Figure. 1.23. Experimental derivation of the phase diagram for a eutectic system of two components A and B with limited miscibility in the solid state.

A remarkable feature of eutectic systems is the circumstance that at a certain temperature T_E (*eutectic temperature*) not two but three phases are in equilibrium with one another, viz. a solid A-rich α-phase, a solid B-rich β-phase, and a liquid phase L (the melt). The equilibrium relation between the three phases is represented in the diagram by a horizontal *tie-line* (also called *eutectic line*) at the level of T_E. Above this line, there are two so-called 2-*phase areas* (α+L) and (β+L) as well as one 1-phase area (L). All three areas join in one point E (the *eutectic point*) on the eutectic line.

Below the eutectic line, there is one 2-phase area ($\alpha+\beta$). To their left, the 2-phase areas border a single-phase area (α) and to their right, they border a single-phase area (β). In the (α+L)-area, the melt is in equilibrium with the solid α-phase and in the (β+L)-area with the solid b-phase. In the ($\alpha+\beta$)-area, the two solid phases α and β are in

equilibrium with one another. No additional solid phases exist. To the right of the binary diagram, the cooling-curves for three different alloys 1, 2, 3 are shown as obtained by thermal analysis. On the cooling-curves for alloys 1 and 2, the *eutectic reaction* shows up in the form of sharp kinks. Below the binary diagram, microstructures of the solidified alloys are shown (schematically).

Alloy 1 of concentration c_E (*eutectic alloy*) remains liquid until it passes the eutectic line. Then, it spontaneously precipitates two different solid phases α and β with concentration c_α and c_β respectively. The separation of the melt takes place according to the eutectic reaction $L \rightarrow \alpha + \beta$. The ratio of the relative amounts of α and β in the microstructure of the solidified alloy is exactly equal to the ratio of distance E - M_2 and distance E - M_1 on the eutectic line.

This relationship follows from a law called *lever-rule of phases* which will be explained in paragraph 1.4.3.

Alloy 2 begins to solidify when passing the borderline between the melt (L) and the (L+β)-area. As temperature falls further, β-crystallites of gradually increasing B-concentration precipitate from the melt, depriving it of B-atoms, according to the reaction $L \rightarrow \beta$. As the alloy passes the eutectic line, the residual melt spontaneously solidifies, precipitating α-crystallites of concentration c_α and β-crystallites of concentration c_β, according to the eutectic reaction $L \rightarrow \alpha + \beta$. Also in this case, the above-mentioned lever-rule of phases applies.

Alloy 3 begins to solidify in a similar fashion as alloy 2, gradually reducing the amount of the remaining melt. But on arrival at the borderline between the (L+β)-area and the (β)-area, the residual melt has disappeared and the alloy is completely solidified as β-phase. On further cooling, the alloy passes the borderline between the (β)-area and the (α + β)-area and is now tending to establish an equilibrium between β-phase and α -phase according to the reaction $\beta \rightarrow \alpha + \beta$. Consequently, α-crystallites precipitate along the grain boundaries of the solid β-structure.

Binary eutectic systems are formed e.g. by the following pairs of metals: Pb-Sn (soldering alloys), and Cu-Ag (brazing alloys). In both cases, the eutectic allows to make alloys that melt at considerably lower temperatures than any of the pure metals they are composed of. *Fig. 1.24* shows the binary system Pb-Sn and two typical microstructures.

In the microstructure at left, the pre-eutectic Sn-rich α-phase stands out as small potato-shaped dark areas embedded in the subsequently formed eutectic. The microstructure at right exhibits a plain eutectic with its typical arrangement of alternating lamellae of α- and β-phase.

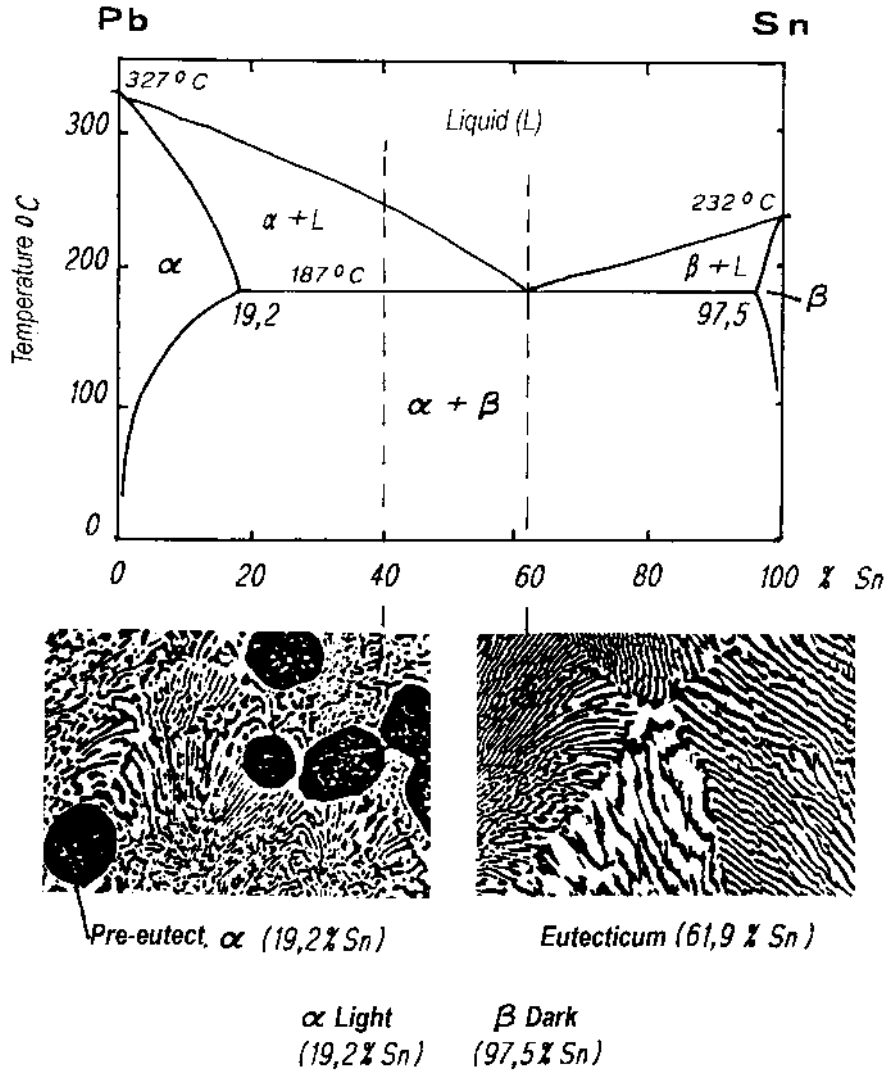

Figure. 1.24. Phase diagram of the system Pb - Sn. Microstructures: α-phase embedded in eutectic (left) and pure eutectic (right).

Peritectic Systems.
An equilibrium between three phases occurs also in a family of binary diagrams called *peritectic*. In these systems, the melt reacts with an already precipitated solid phase, say β, in such a way that a different solid phase, say α, is formed according to the peritectic reaction L+β → α.

Fig. 1.25 shows the binary diagram of a peritectic system and the cooling curves by means of which it is established.

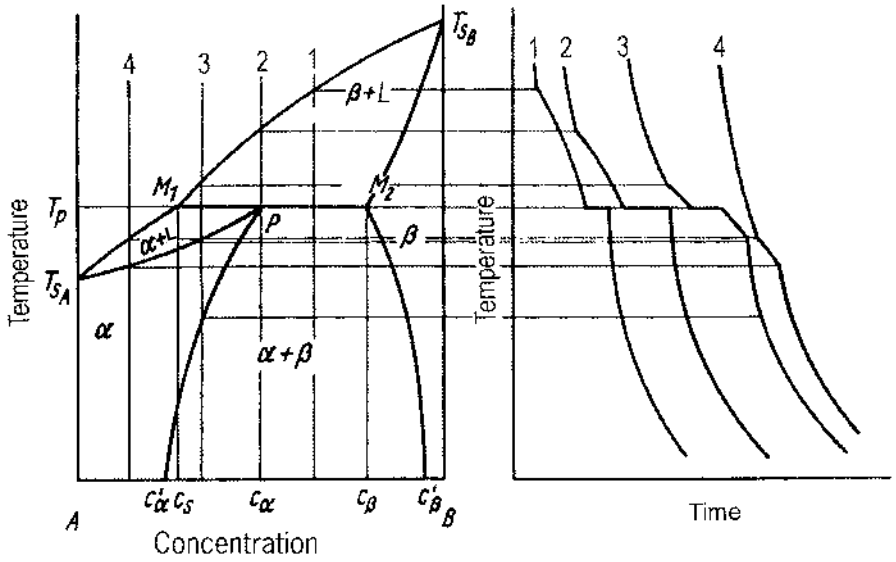

Figure. 1.25. Experimental derivation of the phase diagram of a peritectic binary system A-B.

Eutectoid Systems.
In some binary systems, as for instance in the iron-carbon-system, in addition to the eutectic reaction between the melt and two solid phases L → α + β, an analogous reaction occurs between one solid phase and two other solid phases: γ → α + β which is called *eutectoid reaction*.
The iron-carbon-system is of central interest not only to the metallurgy of conventional steel but also to the powder metallurgy of iron. But before concentrating on this important system, we want to give a more detailed explanation of the above-mentioned *lever-rule of phases* and, in this context, describe the phenomenon of *crystal segregation* which frequently occurs in the solidification process of alloys.

1.4.3 The Lever-Rule of Phases

Guided by the simple binary diagram for two components A and B as shown at *Fig. 1.26*, this rule is readily explained.

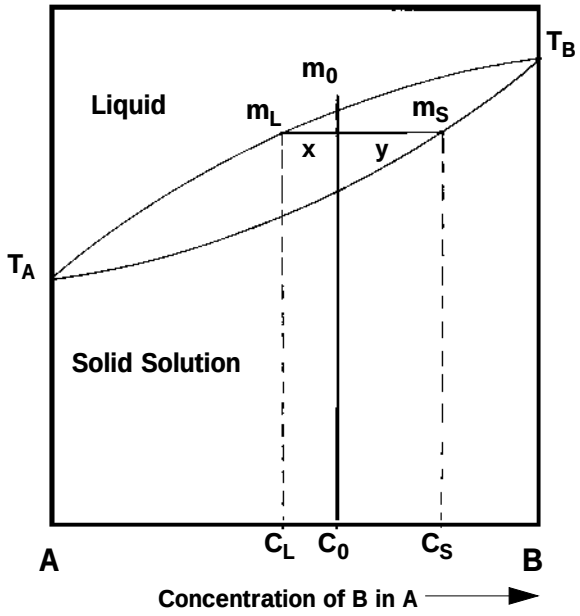

Figure. 1.26. Lever-rule of phases;
m_L = amount of residual melt with concentration c_L.
m_S = amount of solid phase with concentration c_S precipitated from the melt.
$x = (c_0 - c_L)$ and $y = (c_S - c_0)$,
c_0 = initial concentration of the melt = average concentration of the solid alloy.
r-rule: $m_L y = m_S x$.

We assume that a given amount m_0 of a molten alloy of concentration c_0 (concentration of B-atoms) is rapidly cooled down to a point P_0 inside the 2-phase area (liquid + solid). Through P_0 we draw a horizontal line (the so-called *tie-line*) which cuts the two phase-borderlines at the points P_L and P_S respectively. In this undercooled state, the melt of concentration c_0 has become thermodynamically instable.

According to the binary diagram, a melt of concentration c_L should now be in equilibrium with a solid phase of concentration c_S. In order to establish this new equilibrium, crystallites of concentration $c_S > c_0$ must precipitate depriving the melt of B-atoms. In this reaction, both, the total amount $m_0 = (m_L + m_S)$ of alloy and the total amount $c_0 m_0$ of B-atoms must remain unchanged.

Thus, the following two laws apply:

(a) Conservation of total mass: $\mathbf{m_0 = m_L + m_S}$

(b) Conservation of mass of B-atoms: $\mathbf{c_0 m_0 = c_L m_L + c_S m_S}$

Inserting (a) into (b): $\mathbf{m_L (c_0 - c_L) = m_S (c_S - c_0)}$

Evident from the diagram: $\mathbf{x = (c_0 - c_L)}$ and $\mathbf{y = (c_S - c_0)}$

Lever-rule of phases: $\mathbf{m_L x = m_S y}$

m_0 = mass of melt before solidification = total mass of alloy
m_L = mass of residual melt after established equilibrium
m_S = mass of solidified phase after established equilibrium
$c_0 m_0$ = mass of B-atoms before solidification
$c_L m_L$ = mass of B-atoms in residual melt
$c_S m_S$ = mass of B-atoms in solidified phase

The lever-rule of phases expressed in words: (amount of residual melt) x (tie-line from balance point to liquidus line) = (amount of precipitated solid phase) x (tie-line from balance point to solidus line).

1.4.4 Crystal Segregation

Frequently, during solidification of molten alloys, a characteristic phenomenon called *crystal segregation* occurs, i.e. a heterogeneous distribution of concentration inside individual crystal grains of the solidified alloy. Crystal segregation comes about as follows:

As can be seen from the binary diagram shown at *Fig. 1.27*, solidification starts with the precipitation of small B-rich dendrites of concentration $c_1 > c_0$. As solidification continues, thin layers of decreasing concentration of B-atoms are successively being deposited on the dendrites, wrapping them in ”onion skins” so to speak. In the outermost layer, the concentration of B-atoms is $c_n < c_0$. The varying amount of B-atoms in the individual layers is a direct consequence of the above-mentioned lever-rule of

phases. Although the concentration of B-atoms in the core of each crystal grain is higher, and in its outermost zone lower, than the original concentration of the melt, the average concentration of the alloy has not changed during solidification.

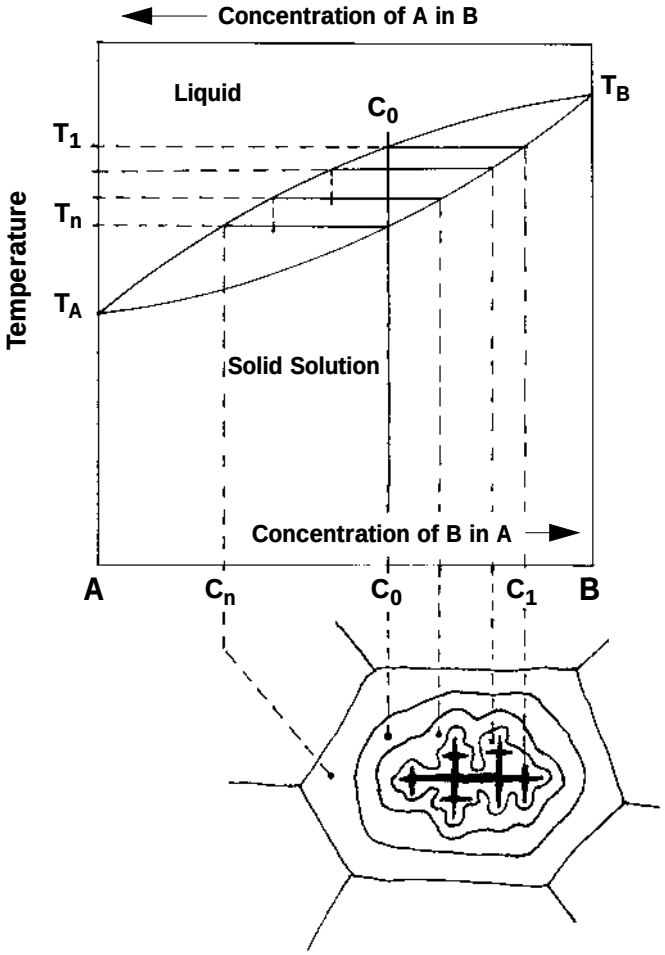

Figure. 1.27. Crystal segregation;
c_0= initial concentration of the melt;
c_1 = concentration of dendritic crystal nuclei first precipitated from the melt;
c_n = concentration of residual melt solidifying last.

When a molten alloy is cooled sufficiently slowly, due to diffusion processes, concentration differences caused by crystal segregation level to a certain degree already during continued cooling. In some cases, in order to improve the properties of the solidified alloy, remaining concentration differences have to be eliminated by means of a subsequent heat treatment called *diffusion annealing* or *homogenizing*.

1.5 The Iron-Carbon System

1.5.1 The Equilibrium Diagram: Iron-Carbon

This binary diagram applies to the *equilibrium states* of carbon-steel and cast-iron. The term *carbon-steel* refers to iron-carbon alloys containing less than approximately 2 %C. The term *cast-iron* refers to alloys containing between 2 and 4 %C where the Fe-C-eutectic occurs. Of interest for technical applications is mainly the iron-rich side of the diagram stretching to the concentration of the inter-metallic phase Fe_3C (6.67 %C).

This part of the diagram is shown at *Fig. 1.28* and can be looked at as being composed of three sub-diagrams: one peritectic, one eutectic and one eutectoid diagram. In connection with the heat treatment of steel, only the eutectoid sub-diagram is of importance. The range up to temperatures of approx. 1150 °C and up to concentrations of approx. 1.5 %C is of particular interest to the powder metallurgy of iron.

Pure iron melts at 1536 °C. Below this temperature, it solidifies in BCC crystal structure, called *δ-iron*, which can dissolve max. 0.10 % carbon interstitially (at 1493 °C). On further cooling, at 1392 °C, δ-iron transforms to FCC crystal structure, called *γ-iron*, which can dissolve max. 2.06 % carbon interstially (at 1147 °C). Carbon-containing *γ-iron* is called *austenite*. At 911 °C, pure *γ-iron* transforms again to a BCC structure, which is called *α-iron* or *ferrite*, and which is *ferro-magnetic* below 723 °C (*Curie-point*). Ferrit can dissolve max. 0,02 % carbon (at 769 °C).

Iron together with carbon forms the *inter-metallic* phase Fe_3C, a carbide called *cementite*, which has an ortho-rombic structure and a carbon content of 6.67 %. Cementite is a so-called *meta-stable* phase because, when annealed for long times at high temperatures, it dissembles into iron and graphite.

Depending on whether carbon occurs bound in cementite or as free graphite, one speaks of the *meta-stable* or of the stable system. Transformations in steel and in white cast-iron proceed according to the meta-stable system (fully drawn lines). Transformations in graphite-containing gray cast-iron proceed according to the stable system (dotted lines).

An austenite containing less than 0.8 %C transforms partly to ferrite when it passes the phase-borderline GS (also called A_3), and below the eutectoid line PS (also called A_1), its residue separates into ferrite and cementite, forming a lamellar structure called *pearlite*. An austenite containing exactly 0.8 %C transforms directly and entirely to pearlite when it passes through the eutectoid point S.

An austenite containing more than 0.8 %C transforms partly to cementite (secondary cementite) when it passes the phase-borderline SE (also called A_{cm}), and below the eutectoid line SK, its residue transforms directly to pearlite.

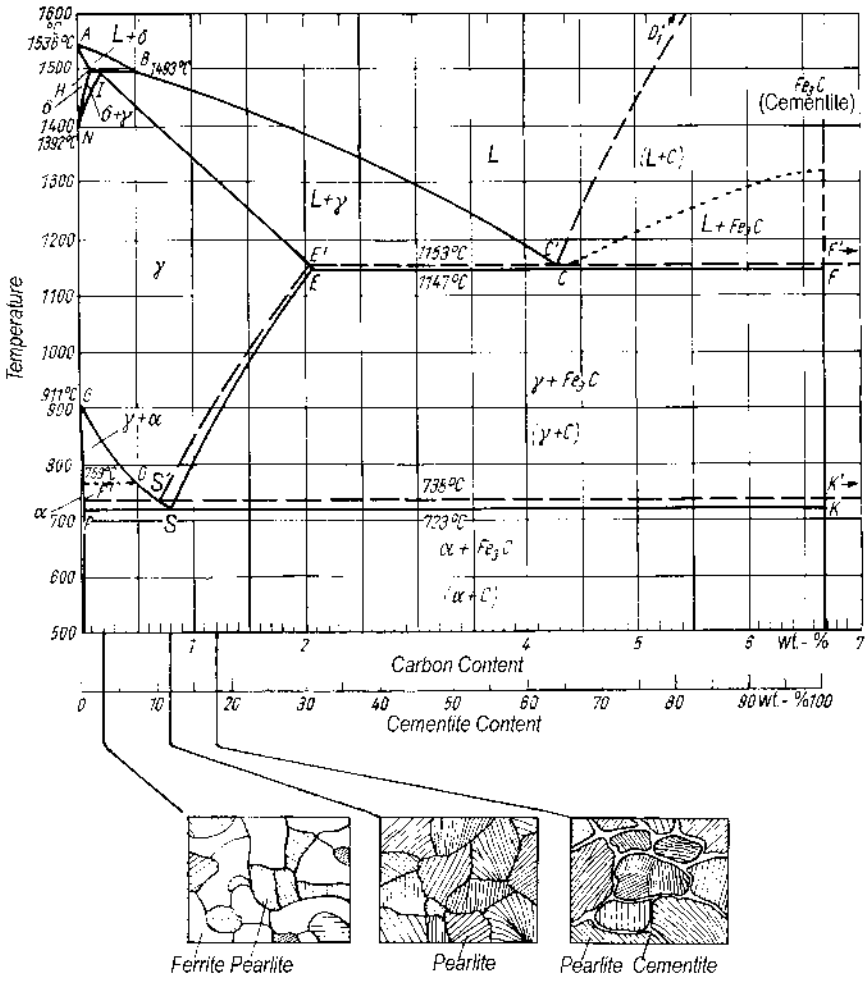

Figure 1.28. Equilibrium phase diagram of the system – Iron-carbon: fully drawn lines = metastable system (Fe-Fe3C), dotted lines = stable system (Fe-graphite).

With reference to these three model cases, one distinguishes between hypoeutectoid, eutectoid (pearlitic) and hypereutectoid iron-carbon-alloys or steels. The respective microstructures are presented schematically below the diagram. Real microstructures of austenite, ferrite, pearlite and cementite are shown at *Fig. 1.29*.

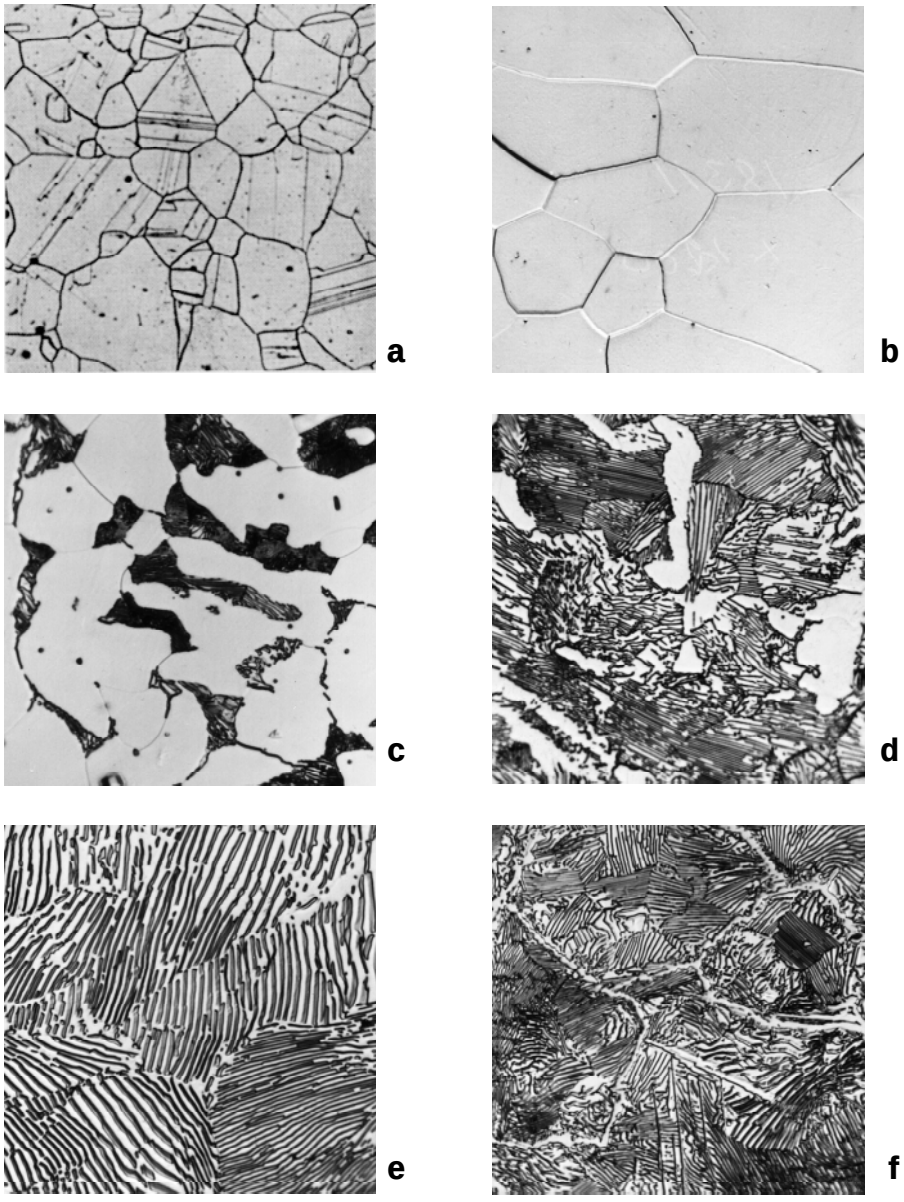

Figure 1.29. Microstructure of steel; a. Austenite (stainless steel), b. Ferrite (< 0,02 % C), c. Ferrite + Pearlite (0,30 % C), d. Pearlite + Ferrite (0,60 % C), e. Pearlite (0,85 % C), f. Pearlite + grain boundary cementite. [1.4]

1.5.2 The Non-Equilibrium Diagram: Iron-Carbon

The iron-carbon diagram as shown at *Fig. 1.28* – like the binary diagrams treated further above – pertain to states of equilibrium and can, in principle at least, be deduced theoretically from classical thermodynamics. With cooling rates as usually practiced in the steel-producing and steel-working industry, states of equilibrium are not always easily achievable and, in many cases not even desirable.

To the contrary, it is just the aimed provocation of certain meta-stable states that offers outstanding technical advantages. With their corresponding microstructures, the value scale of properties like tensile strength, elongation, hardness and toughness can be largely extended. By varying the additional parameters *time* and *cooling-rate*, iron-carbon-based materials can be optimally adapted to a great variety of applications.

At the present state of development of thermodynamic theories, it is still not possible to quantitatively describe the states of non-equilibrium as occurring during forced cooling of steels. Therefore, empirically-experimentally established transformation diagrams are still the only basis on which heat treatments of steel can be intelligently planned.

Such transformation diagrams, known as TTT-diagrams (for Time, Temperature, Transformation), exist today for all common types of steel and can be found in brochures made available by the steel producers. In paragraph 1.6, these diagrams will be discussed in detail.

Transformations in the solid state require rearrangement of atoms by diffusion and in some cases also certain mechanisms of shearinging the crystal lattice. Since diffusion is a time- and temperature-dependent process, the attainment of equilibrium is the more retarded the more the steel is undercooled. At sufficient degrees of undercooling, meta-stable and instable crystal structures (and corresponding microstructures) occur which considerably deviate from equilibrium structures.

With increasing cooling rate, the phase-borderlines in the equilibrium diagram: iron-carbon (Fig. 1.28), are moving towards lower temperatures, particularly the borderlines GSE (A_3) and PSK (A_1) of the austenite area. The diagram at *Fig. 1.30* shows the displacement of the A_3-point and the of the A_1-point with increasing cooling rate for a steel with 0.45 %C. As can be seen from this diagram, the A_3-point moves faster towards lower temperatures than the A_1-point.

As a consequence, with increasing cooling rate, the formation of pre-eutectoid ferrite is more and more reduced and, eventually, entirely suppressed as A_3 and A_1 join in a common A-point. At still higher cooling rates, Bainite (A_B) and Martensite (M_S) are formed.

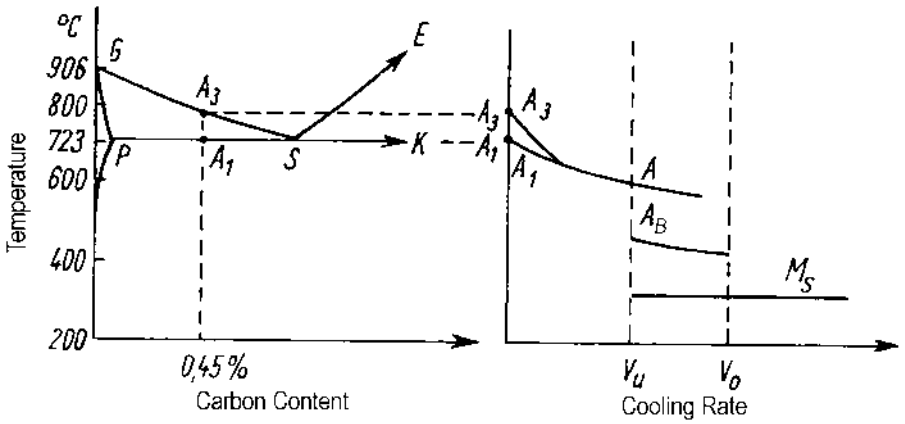

Figure 1.30. Influence of cooling rate on the position of the transition points A_3 and A_1 for a steel with 0.45 % C. [1.5]

The influence of cooling rate on the displacement of A_3 and the A_1, as just described for a steel with 0.45 %C, applies analogously to the entire eutectoid part of the iron-carbon diagram, i.e. to all plain carbon steels.

The diagram at *Fig. 1.31* illustrates the situation. Pertaining cooling rates are stated along the right ordinate of the diagram. With reference to cooling rates, one distinguishes between the following five steps of undercooling:

Undercooling step 0 (equilibrium).
Equilibrium transformation at very low cooling rate.

Undercooling step I.

Already at a cooling rate of 1 Ks^{-1}, a reduced formation of pre-eutectoid ferrite in under-eutectoid steels and of pre-eutectoid cementite in over-eutectoid steels becomes noticeable. At further increased cooling rate, the formation of pre-eutectoid ferrite is gradually hampered to such a degree that it occurs only in steels of very low carbon contents.

The austenite transforms to pearlite of increasingly finer lamellar structure which, when just about resolvable by light-microscopic methods, is called *sorbite*. In hypoeutectoid steels, the formation of pre-eutectoid cementite is completely suppressed.

Undercooling step II.
An extremely fine-lamellar pearlite, called *trostite*, is formed. Its lamellar structure is resolvable by means of electron-microscopic methods only. The united undercooling steps I and II are also called pearlite step.

Undercooling step III.
In this is so-called bainite step (below approx. 450 °C), the diffusion of iron atoms has practically ceased, and a formation of pearlite is no longer possible. Only the interstitial carbon atoms can still diffuse in this temperature range. Already before the BCC austenite lattice shears into the FCC ferrite lattice, cementite begins to precipitate. The resulting microstructure consists of finely dispersed cementite particles in a matrix of acicular ferrite. It is a kind of dispersion-hardened ferrite, so to speak. The orientation of the ferrite needles is related to the initial austenite lattice.

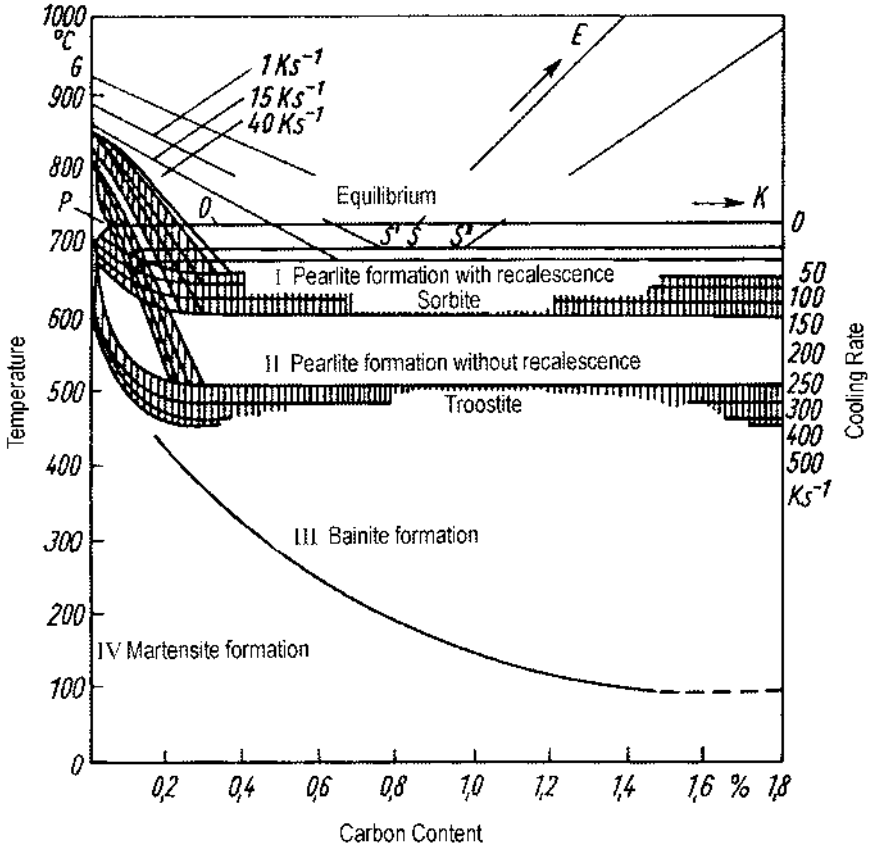

Figure 1.31. Influence of cooling rate on the position of phase boundary lines in the eutectoid part of the Fe- Fe_3C - diagram. [1.6]

Undercooling step IV.
In this so-called martensite step, the undercooling of the austenite is so extreme that the diffusion of carbon atoms has ceased and, hence, the formation of cementite has become impossible. The FCC lattice of the extremely undercooled austenite shears diffusionless into a tetragonally distorted (BCT) ferrite lattice. Since the so formed ferrite is extremely supersaturated with carbon, high internal stresses occur in its lattice. The tetragonal distortion of the lattice and the internal stresses increase with increasing carbon content. *See Fig. 1.32*. This is the cause of the high hardness of martensite.

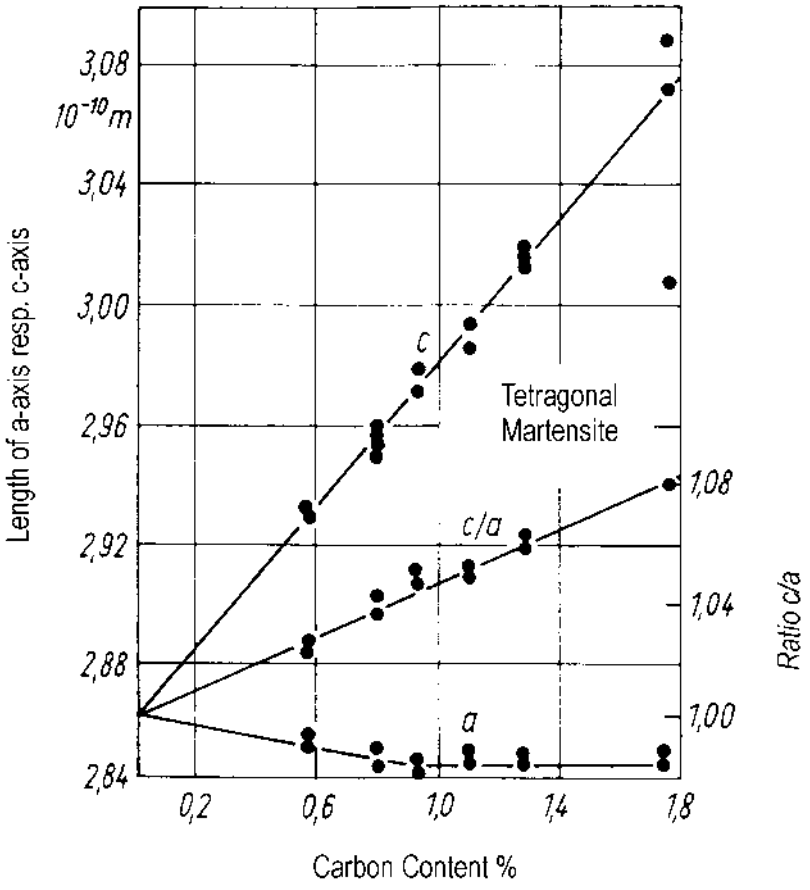

Figure 1.32. Influence of carbon content on the axis lengths of the tetragonal martensite lattice. [1.7]

1.5.3 Mechanisms of Austenite Transformation

To further the understanding of austenite transformations, it will be helpful to discuss in more detail the various mechanisms of diffusion and structural changes involved in the formation of ferrite, pearlite, bainite and martensite.

In between the close-packed iron atoms in the FCC lattice of austenite, there are two types of interstices: the smaller *tetrahedral* and the larger *octahedral* interstices as shown in the schematic diagrams at *Fig. 1.33*. Carbon atoms dissolved in austenite occupy octahedral interstices only, where they cause the least possible lattice distortions and internal stresses. To each unit cell of the austenite lattice belong four octahedral interstices (one at its center and a quarter of one on each of its twelve edges). Thus, in each unit cell, there are four positions available to be filled by carbon atoms. Since also four iron atoms belong to each austenite cell, the theoretically possible concentration of carbon atoms in austenite would be 50 at.-% compared to their maximal concentration of 9.51 at.-% in reality. This means that, even at maximal carbon concentration, most octahedral interstices in the austenite lattice remain unfilled.

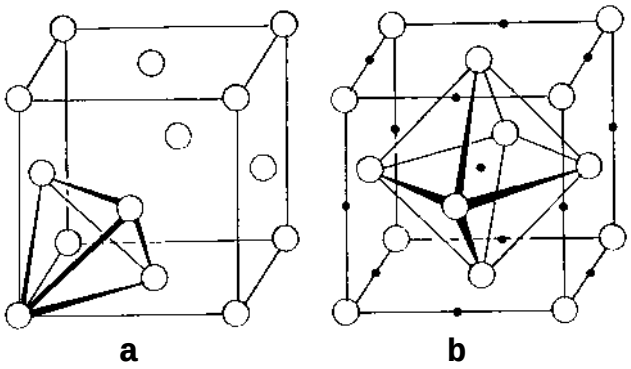

Figure. 1.33. Tetrahedral (a) and octahedral (b) interstices in the FCC lattice of austenite.
• = possible sites of carbon atoms.

Ferrite Formation.
Pure γ-iron does not contain any carbon atoms at all. In hypoeutectoid steels (< 0.8 wt.-% = 3.7 at.-%), at best, only one out of seven unit cells of austenite contains one carbon atom. Between 911°C and 723°C, because of the sparse distribution of carbon atoms, parts of the FCC austenite lattice can easily shear into the BCC ferrite lattice, while carbon atoms, not dissolvable in ferrite, get enriched in the residual parts of the austenite. This shearing mechanism requires a minimum of rearrangement of iron atoms in the respective crystal lattices, as becomes evident from the schematic diagram at *Fig. 1.34*. In the drawing representing two adjacent FCC cells, certain iron-atoms

(filled circles) are connected by tie-lines in such a way that they form a body-centered-tetragonal (BCT) cell. It does not take much imagination to comprehend that a slight stretching of its horizontal and/or slight upsetting of its vertical edges turns this BCT cell into an ordinary BCC cell. The theoretically possible positions of carbon atoms are indicated by small black spots on the edges of the cell. Since the described shearing mechanism occurs almost instantly, one could say that, on cooling, the FCC lattice of austenite "snaps" into the BCC lattice of ferrite (or vice versa on heating).

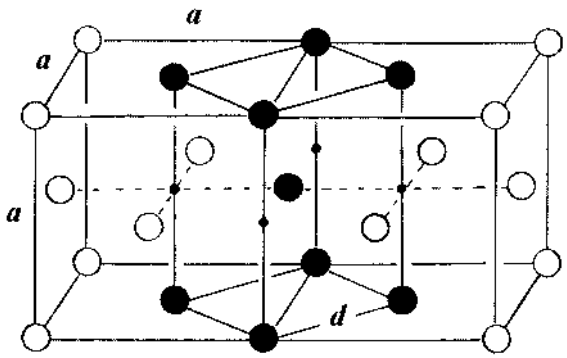

$$a = d\sqrt{2}$$

Figure. 1.34. Geometrical interrelation between the FCC lattice of austenite and the BCC lattice of ferrite. • = possible sites of carbon atoms.

Cementite Formation.

The maximal solubility of carbon in austenite is 2.06 wt.-% = 9.51 at.-% and occurs at 1147°C (eutectic temperature). This means that scarcely twenty percent of all theoretically possible positions are filled with carbon atoms (i.e. less than one carbon atom per austenite cells). A denser filling with carbon atoms (supersaturation) would increase internal stresses in the austenite lattice to such extend, that the corresponding increase in elastic energy would exceed the formation energy of cementite.

Consequently in case of supersaturation with carbon, the austenite tends to lower its free enthalpy by transforming to cementite. The tendency increases with increasing degree of undercooling. The concentration of carbon in cementite is 25 at.-%, i.e. at least close to three times higher than in austenite. Thus, in order to form cementite, considerable amounts of carbon atoms must be adequately displaced by diffusion.

Not enough with carbon diffusion, – iron atoms too must be rearranged by diffusion in order to enable the austenite to transform partly into cementite. Thus, the formation of cementite depends not only on the austenite's opportunity to lower its free enthalpy but also on the actual mobility of the carbon atoms (which decreases with

increasing degree of undercooling). At temperatures where the mobility of carbon atoms in the austenite lattice has ceased, cementite cannot be formed, and martensite occurs instead. See further down.

Pearlite Formation.
Below the eutectoid temperature (723°C), austenite separates into cementite and ferrite, thereby lowering the free enthalpy of the alloy. Nucleated at the austenite grain-boundaries, lamellas of cementite and ferrite grow side by side gradually towards the center of the austenite grains as shown in the schematic diagrams at *Fig. 1.35*. The lamellar structure occurs because the precipitating cementite completely deprives its austenitic neighborhood of carbon triggering it's transformation to ferrite. With increasing degrees of undercooling, i.e. decreasing temperature, the diffusion rate of carbon decreases and, consequently, the lamellar structure of the pearlite becomes finer (and harder).

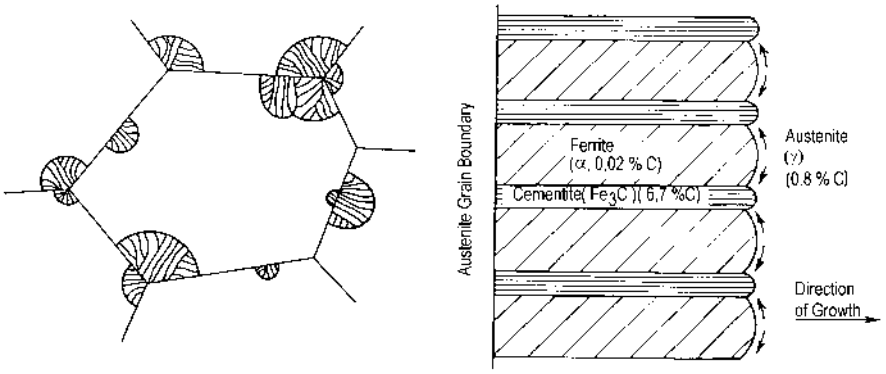

Figure 1.35. Nucleation of pearlite colonies at austenite grain boundaries (left) and growth of pearlite lamellas in austenite grains (right). [1.8]

Martensite Formation.
Martensite formation is based on the same mechanism as ferrite formation. The difference lies in the cooling rate. At low cooling rates, carbon atoms have sufficient time to diffuse and form cementite before the lattice of the residual austenite shears into the ferrite lattice. At very high cooling rates, as in quenching procedures, carbon atoms cannot move fast enough to avoid getting trapped inside the spontaneously forming ferrite. Since ferrite, under equilibrium conditions, cannot dissolve more than 0.02 wt.-% = 0.09 at.-% carbon, it is now extremely supersaturated with carbon, and its

lattice correspondingly (tetragonally) distorted (ref. Fig 1.32).
The high internal stresses arising from this distortion are the cause of the high hardness of martensite. In microstructures, the tetragonally distorted ferrite, i.e. martensite, appears in the form of relatively coarse needles oriented at certain angles inherited from the initial austenite lattice.

The small areas in between the needles are residual austenite. See micrograph at *Fig*. 1.36 a. When annealing martensite at temperatures above M_S , finely dispersed cementite precipitates from the supersaturated ferrite. See micrograph at *Fig. 1.36 b*. Thus, the high level of internal stresses in the tetragonal ferrite lattice is reduced, and the brittleness of the martensite correspondingly lowered.

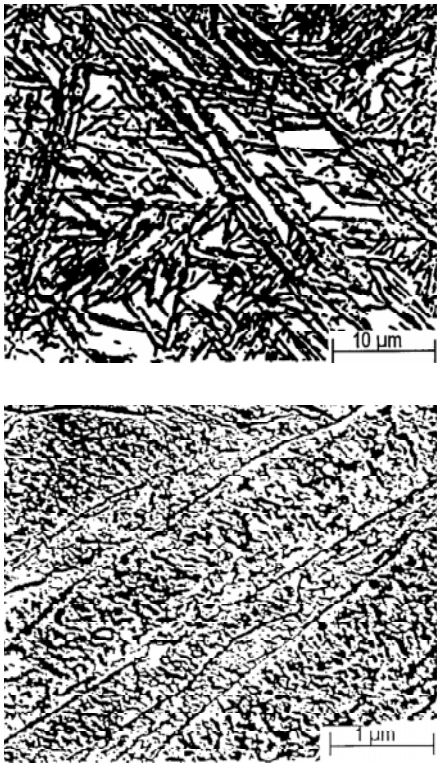

Figure. 1.36. Acicular martensite (a) and tempered martensite with finely dispersed cementite (b). [1.9]

Bainite formation.
Bainite is of great technical interest because it offers a very favorable combination of hardness and toughness not easily attainable with martensite. According to differences in cooling conditions, one distinguishes between two kinds of bainite: *upper bainite* and *lower bainite*.

Upper bainite occurs at temperatures around 500 °C where diffusion rates of carbon are relatively higher. Lower bainite occurs at temperatures around 300 °C (but above M_S) where diffusion rates of carbon are relatively lower.

In the case of upper bainite, small parallel ferrite platelets, nucleated by shearing processes, grow gradually inside the austenite. Moving ahead of the growing ferrite platelets, carbon atoms accumulate in the residual austenite which gets increasingly more restricted. Eventually, the residual austenite becomes so restricted and so much enriched in carbon that it transforms to cementite jammed between the ferrite platelets. See micrograph at *Fig. 1.37a*.

In the case of lower bainite, ferrite platelets form in much the same way as in upper bainite but faster. At the same time, the diffusion rate of carbon has dropped so much that carbon atoms cannot move fast enough to avoid getting trapped inside the fast growing ferrite platelets. In this respect, the mechanism of lower bainite formation is quite similar to the mechanism of martensite formation.

But in the case of lower bainite, temperatures are high enough to initiate precipitation of finely dispersed cementite particles inside the ferrite platelets immediately after they have been formed. See microstructure at *Fig. 1.37 b*. One could say that lower bainite is a kind of self-tempered martensite. Indeed, comparing *Fig. 1.36 b* with *Fig. 1.37 b*, it can be seen that the microstructures of lower bainite and tempered martensite have a certain resemblance.

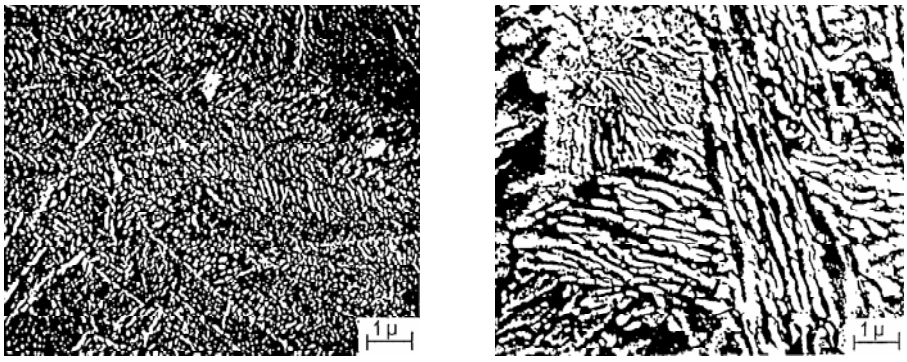

Figure 1.37. Lower (a) and upper (b) bainite in a bainitic steel (0,87 % C; 0,44 % Mn; 0,17 % Si; 0,21 % Cr; 0,39 % Ni). [1.10]

1.6 Transformation Diagrams of Steels

As briefly mentioned in paragraph 1.5.2, the goal of commercial heat treatment of steel is attaining optimal combinations of properties adaptable to a large variety of applications. This can only be achieved by steering the formation of adequate microstructures via strictly controlled cooling rates and holding times.

Adequate heat-treating procedures cannot be designed on the basis of equilibrium diagrams. To this end, a particular kind of empirically established transformation diagrams are required, usually called *Time-Temperature-Transformation* diagrams, or *TTT-diagrams* for short. According to the procedure by which they are established, one distinguishes between Isothermal Transformation diagrams (*ITT-diagrams*) and Continuous Cooling Transformation diagrams (*CCT-diagrams*).

We concentrate our interest mainly on ITT-diagrams, since these are usually better suited for the planning of reliable heat-treating procedures than CCT-diagrams (apart from the fact that the latter are of limited availability). ITT-diagrams are today available for practically all common types of steel and can be found e.g. in brochures edited by steel-makers.

Before going into details, a general feature of phase transformations must be briefly explained. Phase transformations in metals (like any kind of phase transformations) pass through two characteristic periods: a period of nucleation and a period of growth. Nucleation is a process in which small nuclei of a new phase precipitate at random from the ”mother”-phase. Growth means that nuclei, which incidentally exceed a critical minimum size, begin to grow on account of the mother-phase, eventually replacing it entirely.

The growth rate of the new phase is proportional to the residue of untransformed mother-phase, i.e. at the beginning, the new phase grows fast, but as the amount of mother-phase shrinks, the growth rate of the new phase slows down accordingly. This mechanism yields the characteristic s-shaped transformation curve as shown schematically at *Fig. 1.38*.

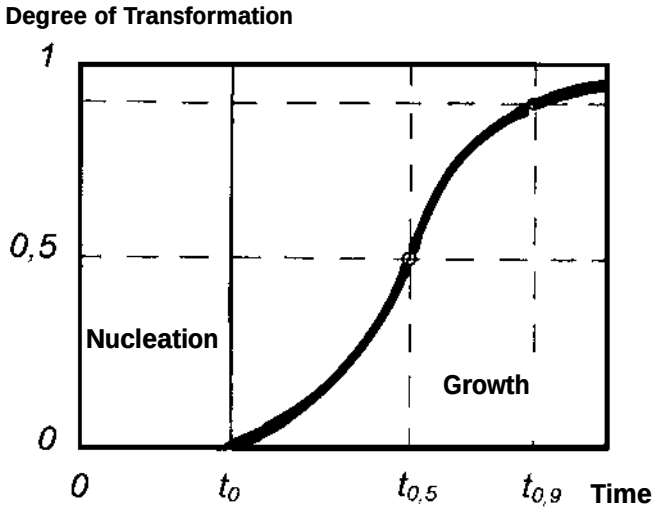

Figure 1.38. Typical s-shaped course of isothermal transformation passing from a period of nucleation to a period of growth.

1.6.1 ITT-Diagrams

In order to experimentally derive an ITT-diagram, a series of small specimens of the steel to be investigated are austenitized at a temperature above A_3. From austenitizing temperature, the specimens are individually quenched to certain pre-selected temperatures, where they are held for various lengths of time. Subsequently they are quenched to R.T. On the so-treated specimens, the amount of residual austenite is determined by means of quantitative metallographic methods. Plotting the so-obtained amounts of residual austenite against respective holding times, characteristic s-curves (of type as discussed above) emerge – one for each holding temperature. On each of these curves, three points of time are marked:
1) the point of beginning transformation (100 % austenite),
2) the point where the amount of residual austenite has decreased to 50 % (50 % transformation) and
3) the point where the amount of residual austenite has dropped to 10 % or less (90 - 100 % transformation). Transferring these three points from each individual S-curve to a temperature-time-diagram, as illustrated schematically at *Fig. 1.39*, one obtains an ITT-diagram with three characteristic ”nose”-shaped curves, representing begin, half-completion and end of austenite transformation respectively.

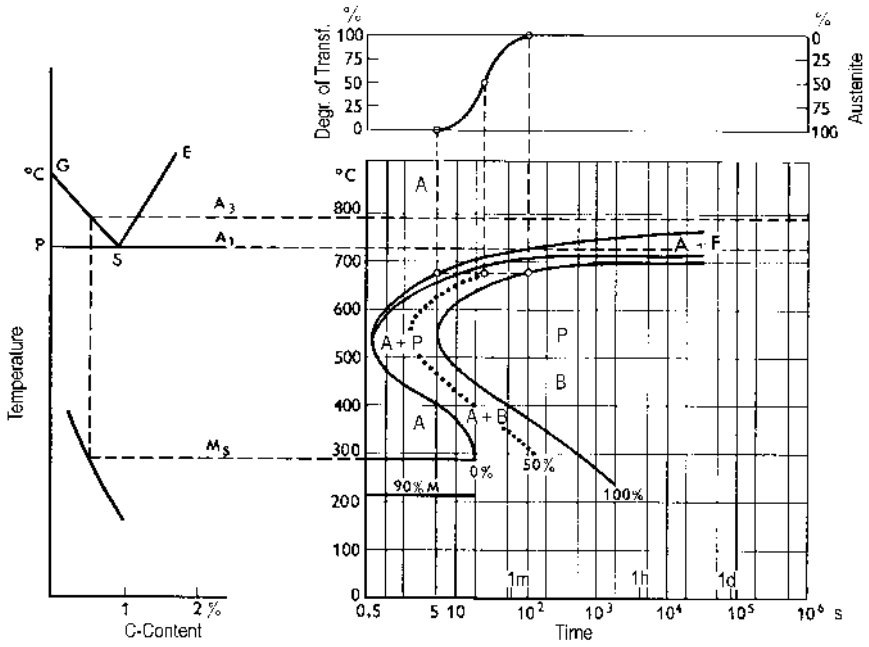

Figure 1.39. Empirically derived ITT-diagram for a hypoeutectoid carbon steel (right) and its relation to the equilibrium phase diagram Fe-Fe_3C (left). Austenitizing above A_3. A = austenite, F = ferrite, P = pearlite, B = bainite, [1.11]

The following details are noted:

- At low degrees of undercooling, i.e. at temperatures close below A_1, rather long periods of time elapse before transformation begins (hours or days). Transformation product: pearlite (P) and residual austenite (A).
- With increasing degrees of undercooling, transformation begins correspondingly sooner. Transformation product: P + A.
- At medium degrees of undercooling, i.e. at temperatures between approx. 550 and 500 °C, transformation begins almost instantly (after less than 1 second). Transformation product: P + A.
- With further increasing degrees of undercooling, the begin of transformation is delayed again (up to approx. 20 seconds). Transformation product: A + B (bainite).

- At quenching to temperatures below approx. 280 °C, large parts of austenite transform instantly (without preceding period of nucleation) into martensite (M). The lower the quenching temperature, the smaller is the amount of residual austenite. Transformation product: x% A + (100 - x)% M.

The nose of the transformation curves between 500 and 600 °C is called *pearlite-nose* because above its tip, austenite transforms to pearlite. The nose-shape of the transformation curves has a simple explanation. Close below A_1, the diffusion rate of carbon is high, but, due to the low degree of undercooling, the probability of cementite nucleation is very low. With increasing degrees of undercooling, the probability of cementite nucleation increases accordingly, but the diffusion rate of carbon decreases. As a result of these two counteracting processes, transformation times adopt a minimum between low and high degrees of undercooling.

Carbon steels with less than 0.25 %C are not well suited for heat-treating procedures aiming at the formation of martensite or bainite. Their pearlite-nose lies too far left in the ITT-diagram and cannot be bypassed at technically practicable cooling rates.

A cooling curve just touching the pearlite-nose is called *critical cooling curve*. When the carbon content is increased or when alloying elements like Cr, Ni, Mn, Si, or W are added, the pearlite-nose is shifted toward the right in the diagram, the critical cooling rate is correspondingly decreased, and the formation of martensite and bainite facilitated.

Certain combinations of Cr-, Ni-, Mn-, and Mo-additions entail transformation curves with two noses. Underneath the pearlite-nose a so-called *bainite-nose* occurs as in the ITT-diagram shown at *Fig. 1.40*.

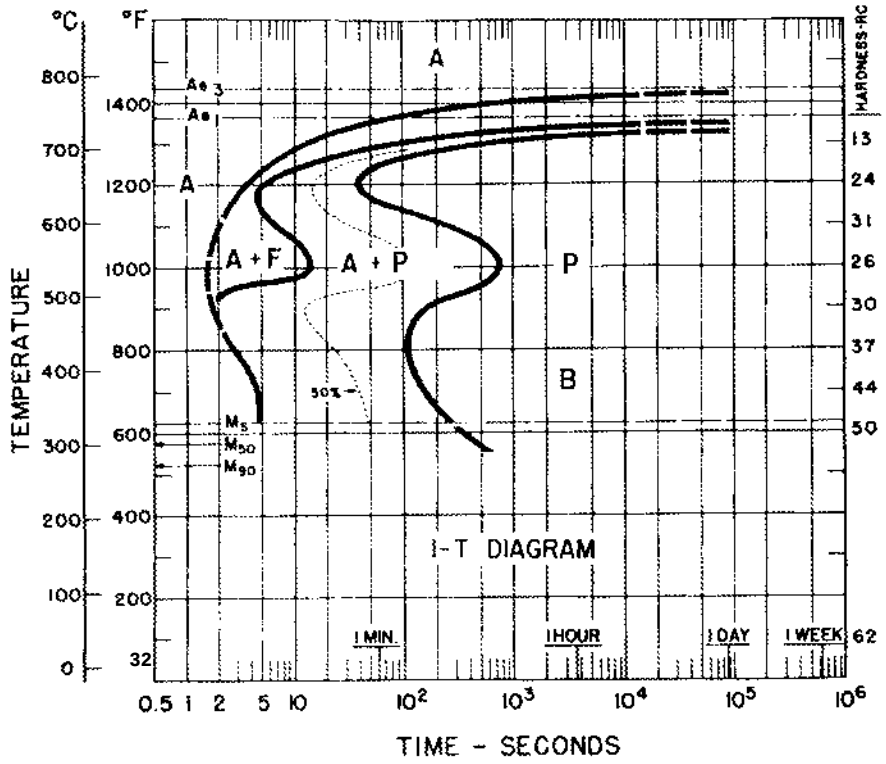

Figure 1.40. ITT-diagram with pronounced ”bainite-nose” for a steel with 0,42 % C; 0,68 % Mn; and 0,93 % Cr. [1.12]

When cooling a big work piece of steel from austenitizing temperature, center and surface are cooling at different rates. Then, it may happen that the cooling curve pertaining to the surface bypasses the pearlite-nose, while the curve pertaining to the center passes through it. In such a case, a martensitic microstructure occurs at the surface and a pearlitic-bainitic microstructure at the center of the piece.

See schematic diagram at *Fig. 1.41*. An analogous problem arises, when a heat of smaller pieces is cooled, because pieces located in the outer parts of the heat are cooling faster than those buried deeper inside. This kind of problem is avoided if the heat is quenched to a temperature somewhat above martensite formation (M_S) and held there until transformation is complete.

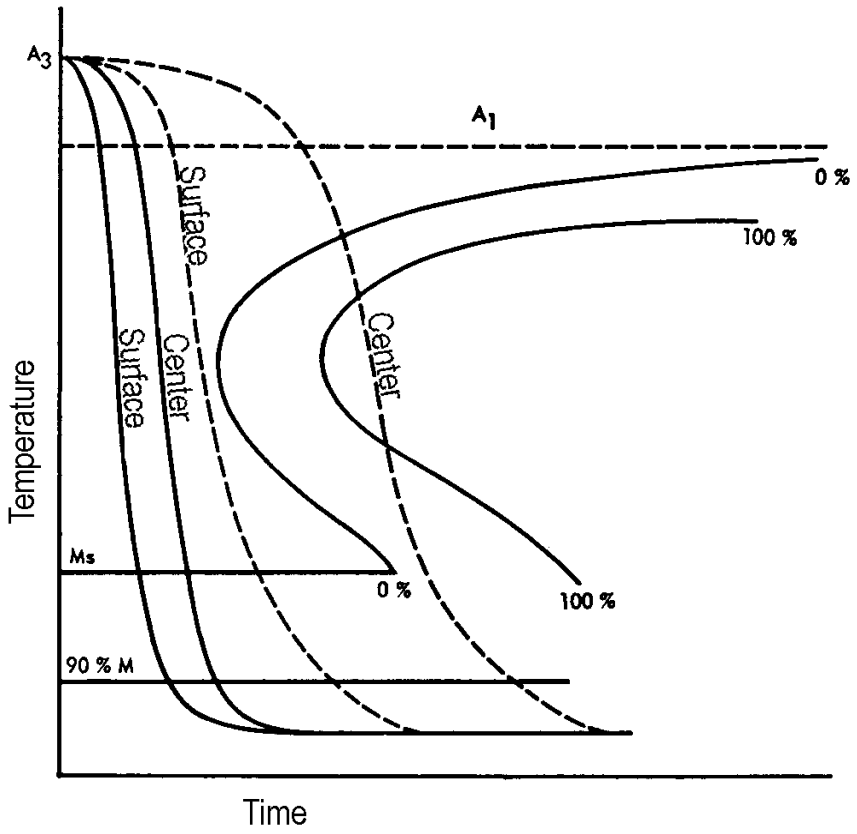

Figure 1.41. Cooling curves for surface and center of a small (fully drawn lines) and of a big (dotted lines) work piece (schematically). [1.13]

1.6.2 Heat Treatment of Steel based on ITT-Diagrams

The properties of steel can be improved considerably through special heat treatments, i.e. certain sequences of heating, quenching and tempering. Properties like strength, hardness, toughness and ductility, depend essentially, if not entirely, on the microstructure of the steel. Heat-treating procedures must, therefor, be especially designed to attain the required microstructures.

For the design of reliable heat treatments, ITT-diagrams are indispensable.

Depending on the kind of application, one or the other of the following four standard heat treatments are frequently applied:

a) Quenching and tempering.
b) Martempering.
c) Austempering (Bainitizing).
d) Isothermal soft-annealing.

The schematic ITT-diagrams shown at *Fig. 1.42* illustrate these procedures which, in detail, can be described as follows:

a) Quenching and tempering:

On quenching to temperatures well below the martensite temperature (M_S), the austenite transforms to a structure consisting of martensite and smaller amounts of residual austenite. In this condition, the steel is extremely hard but also extremely brittle. In order to reduce its brittleness and increase its toughness, the steel is subsequently tempered at temperatures above M_S. Due to temperature differences between surface and core or between thinner and thicker sections of the steel piece, cracks may arise on quenching. Hence, this type of heat treatment is less suited for big work pieces or pieces of complicate shape.

b) Martempering:

In this heat treating process, the risk of crack formation in the steel is avoided. The steel is quenched in a bath at a temperature slightly above M_S and held in the bath until the core of the piece reaches bath temperature. During this period, the bath temperature falls gradually below M_S, and the austenite transforms uniformly into martensite, whereupon the steel is removed from the bath and allowed to cool in air. Subsequently the steel is tempered to desired hardness.

c) Austempering:

In this heat treatment, the steel is quenched to a temperature below the bainite-nose but above M_S, at which temperature the austenite is transformed isothermally to bainite. Subsequent tempering is not required, since, even without tempering, bainite offers a favorable combination of hardness and toughness.

d) Isothermal annealing:

In many alloyed steels, there is a pronounced minimum in the ending line of the ITT-diagram at relatively high temperatures. Assuming that a soft ferritic-pearlitic

structure is to be obtained, advantage may be taken of the time-temperature coordinates of this minimum to design a short annealing cycle. This is accomplished by cooling the steel initially in the austenitic state as rapidly as convenient to the temperature of the minimum and holding it approximately at this temperature for the time required to transform the austenite completely. Subsequently, the steel may be cooled as convenient.

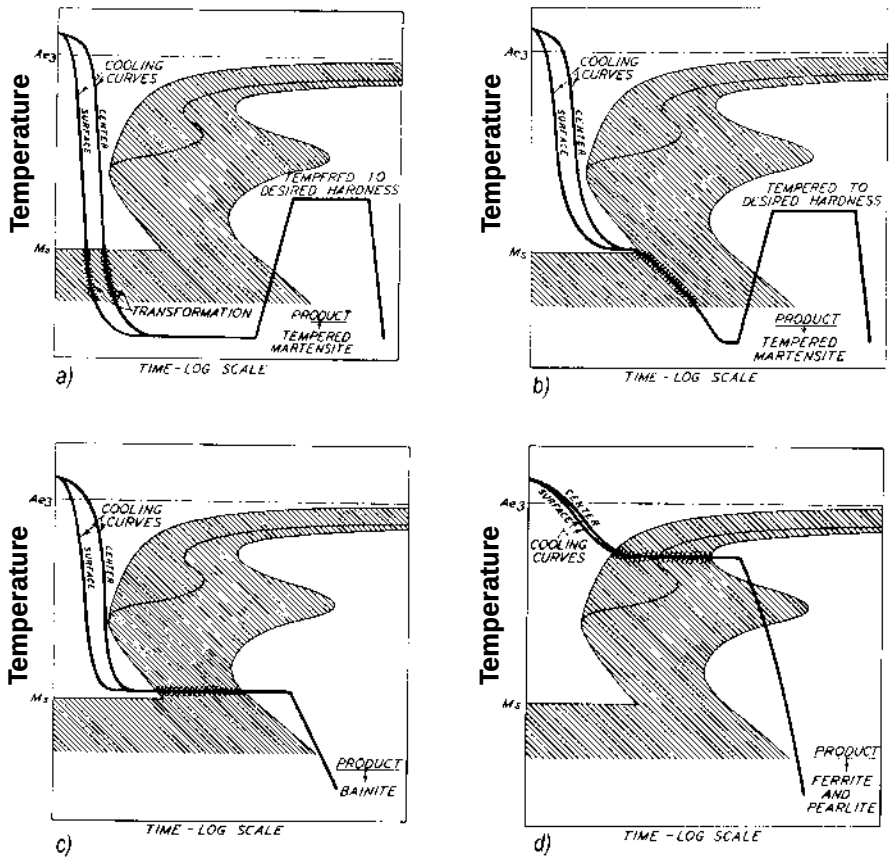

Figure 1.42. Four standard procedures for the heat treatment of steels: a. Quenching and Tempering; b. Martempering; c. Austempering; d. Isothermal Annealing. [1.14]

These examples have shown that ITT-diagrams are helpful guides in designing adequate heat treating procedures. In industrial practice, heat treatments rarely proceed under strictly isothermal conditions. In many cases, continuous cooling procedures are even more practicable. Thus, one might think that CCT-diagrams would be more adequate. But the derivation of CCT-diagrams is a rather tedious task, and would, even if feasible, rarely be warranted since a particular CCT-diagram exactly presents but one sample; samples from other heats, or even from other locations of the same heat, are likely to have slightly different CCT-diagrams.

Thus, when used with discrimination and with its limitations in mind, the ITT-diagram is most useful in interpreting and correlating observed phenomena on a rational basis, even though austenite transforms during continuous cooling rather than at constant temperature.

Fig. 1.43 shows how the CCT-diagram for a typical structural steel is correlated with the corresponding ITT-diagram and with end-quench hardenability. The essential difference between the two transformation diagrams is that, in the CCT-diagram, pearlite-nose and bainite-nose are shifted to lower temperatures and longer transformation times.

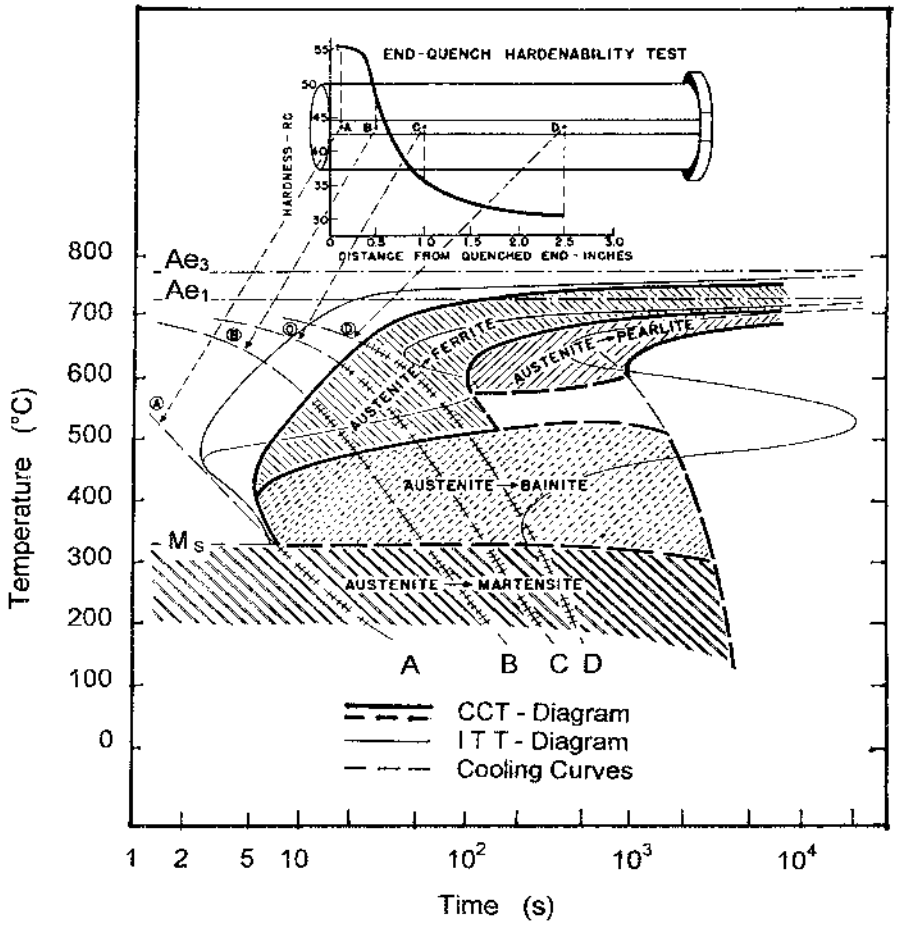

Figure 1.43. CCT-diagram (thick lines) as related to corresponding ITT- diagram (thin lines) and to EQ-hardenability curves (top) for a steel containing 0,37 % C; 0,77 % Mn; 0,98 % Cr; and 0,21 % Mo. Transformation products: (A) martensite, (B), (C), (D) martensite + ferrite + bainite. [1.15]

1.7 Influence of the Microstructure on the Properties of Steel

1.7.1 Pearlite and Spheroidite

In pearlitic structures, lamellas of soft ferrite alternate with lamellas of hard cementite. Under the influence of shearing stresses, plastic deformation occurs essentially only in the soft ferrite lamellas where dislocations can move relatively easily. The thinner the ferrite lamellas are, the more restricted, by the rigid cementite lamellas, is the mobility of the dislocations. This explains why the ductility of pearlite increases and its hardness correspondingly decreases with the thickness of its ferrite lamellas as shown in the diagram at *Fig. 1.44.*

By means of elongated soft-annealing, the cementite lamellas can be spheroidized. In the so transformed pearlite, also called *spheroidite*, small spherical cementite particles are embedded in a coherent ferrite matrix. See microstructure at *Fig. 1.45.*

Spheroidite is the most ductile variety of pearlite because, in its coherent ferrite matrix, dislocations can move more freely, restricted only to a lesser degree by the spherical cementite inclusions.

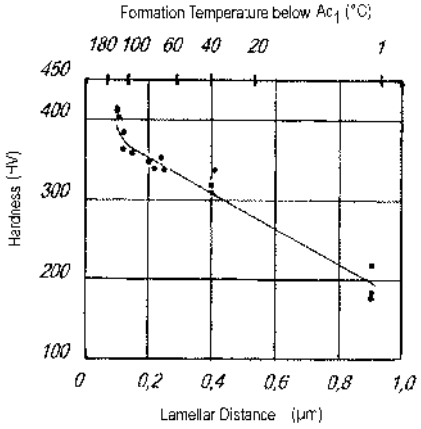

Figure. 1.44. Hardness of pearlite as a function of the distance between its lamellas.

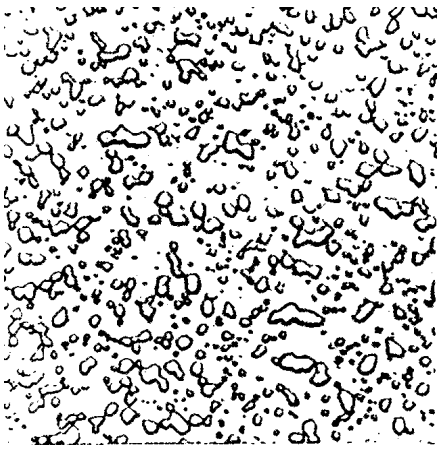

Figure. 1.45. Spheroidized pearlite (spheroidite) in a carbon steel with 1,30 % C.

See diagrams at *Fig. 1.46.* In mixed structures of pearlite and ferrite, strength and hardness increase with increasing proportion of cementite, while toughness and ductility decrease. See diagram at *Fig. 1.47.*

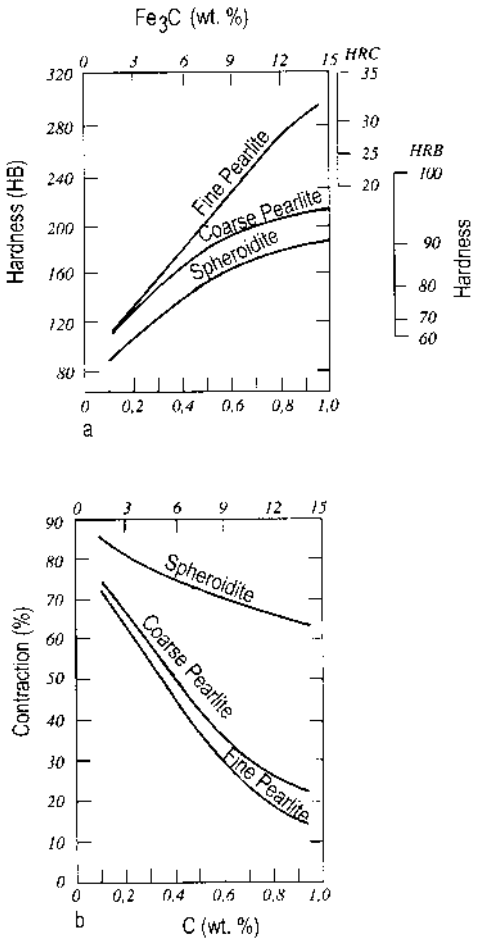

Figure. 1.46. Influence of carbon content on hardness (a) and ductility (b) for a plain carbon steel having fine and coarse pearlitic as well as spheroiditic microstructures. [1.16]

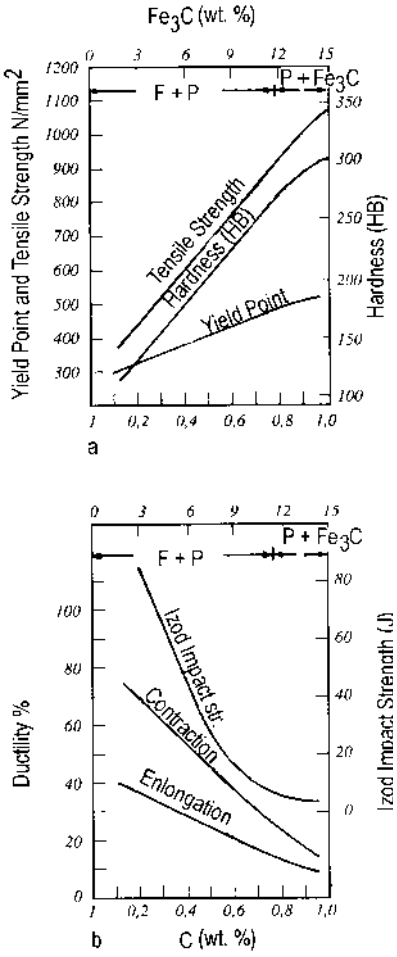

Figure. 1.47. Influence of carbon content on the mechanical properties of a plain carbon steel having a fine pearlitic microstructure. [1.17]

1.7.2 Martensite and Bainite

Martensite is the hardest and most brittle of all phases occurring in microstructures of steel. It has virtually no ductility at all. Its hardness increases with increasing carbon content - first faster (up to approx. 0.4 %C) then slower, approaching a maximum at approx. 1 %C. The diagram at *Fig. 1.48* shows the influence of carbon content on the hardness of martensite and pearlite.

Martensite owes its high hardness not to the presence of cementite, as is the case with pearlite, but to the high internal stresses caused by its supersaturation with carbon. In its heavily distorted crystal lattice, the number of sliding systems available for plastic deformation is extremely low.

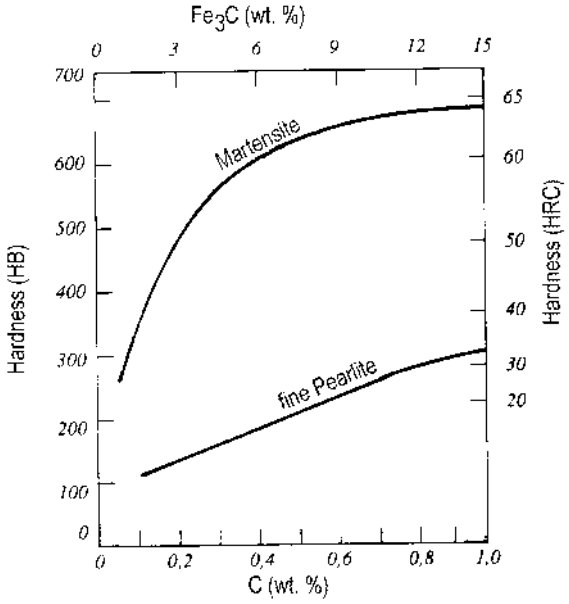

Figure. 1.48. Influence of carbon content on hardness for plain carbon martensitic and fine pearlitic steels. [1.18]

Since austenite has a higher density than martensite, a noticeable volume-increase occurs on quenching. Due to the accompanying shearing stresses, big or intricately shaped work pieces may crack when quenched. This constitutes a serious problem in the heat treatment of steels containing more than approx. 0.5 % C.

In the quenched state, martensite is too hard, too brittle and too crack-sensitive for most applications. Its brittleness can be reduced and its toughness considerably increased through tempering at temperatures between 250 and 650 °C. Internal stresses in the martensite lattice dissolve already at approx. 200 °C. During tempering, carbon atoms

have sufficient time to diffuse and form cementite which precipitates in the form of finely dispersed particles inside the martensite needles (ref. Fig. 1.36 b). Tempered martensite has a certain resemblance to lower bainite (ref. Fig. 1.37 b). The size of the precipitated cementite particles in martensite increases with tempering time and temperature.

By means of varying these two parameters, the properties of hardened steel can be optimally adapted to many different applications. The diagrams at *Fig. 1.49* and *Fig. 1.50* illustrate these possibilities.

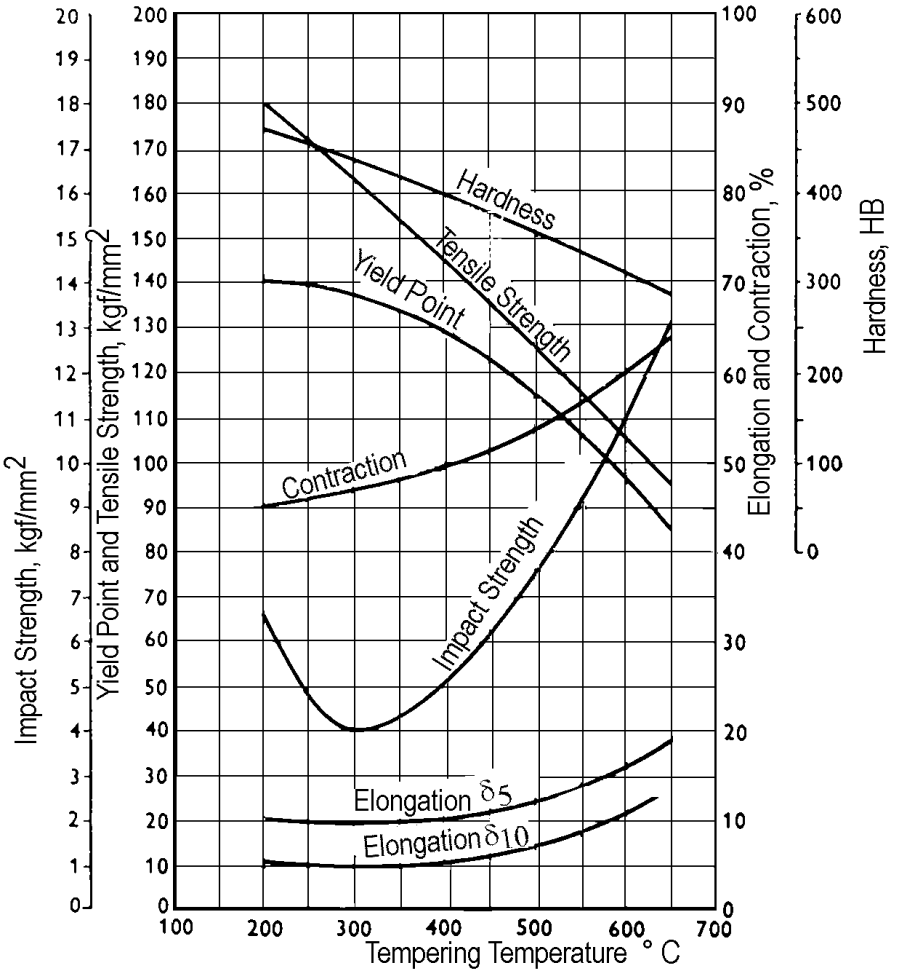

Figure 1.49. Mechanical properties as functions of tempering temperature for a steel, quenched from 850 °C in oil, and containing 0,30 % C; 0,25 % Si; 0,60 % Mn; 0,30 % Cr; 3,30 % Ni and 0,25 % Mo. [1.19]

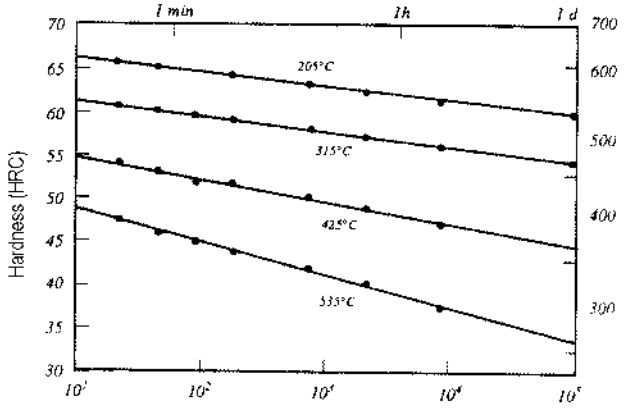

Figure. 1.50. Hardness as a function of tempering time and temperature for a water-quenched eutectoid plain carbon steel. [1.20]

Since the microstructure of bainite - similar to that of tempered martensite - is composed of finely dispersed cementite particles in a ferritic matrix, bainitic steels offer favorable combinations of hardness, strength and toughness.

The diagram at *Fig. 1.51* shows the influence of transformation temperature on microstructure and tensile strength of a low-carbon bainitic steel.

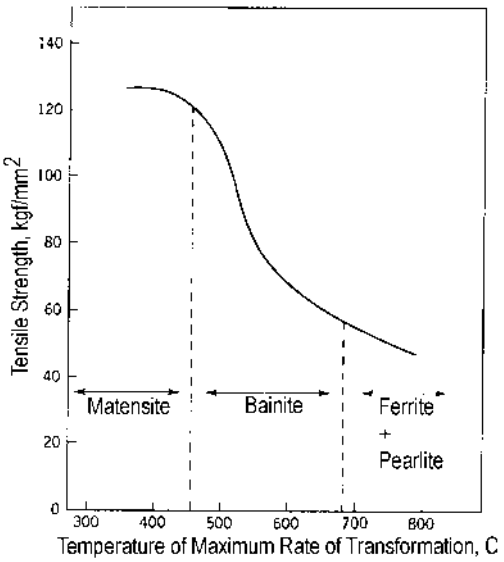

Figure. 1.51. Relationship between temperature of maximum transformation rate and strength of low carbon bainitic steels. [1.21]

1.7.3 Temper Brittleness

With some types of steel, tempering may cause a marked decrease of impact strength. This phenomenon, which is called *temper brittleness*, occurs either when the steel is tempered above 575 °C and subsequently slow-cooled to R.T., or when tempered between 375 and 575 °C. Steels containing Mn, Cr or Ni and, in addition, small amounts of impurities, like Sb, P, As or Sn, are especially sensitive to temper brittleness.

When the mentioned alloying elements and impurities are present, the border between tough and brittle tempered martensite is shifted noticeably to higher temperatures. Crack propagation in temper-brittle steel proceeds along former austenite grain boundaries where the impurities preferentially have segregated during solidification of the melt. Temper brittleness can be avoided by reducing the amount of impurities or by tempering above 575 °C or below 375 °C with subsequent quenching to R.T.

References

[1.1] E. Hornbogen, Symposium: Steel-Strengthening Mechanisms, Zurich, May 5th and 6th 1969.

[1.2] G.E.R. Schulze: Metallphysik, Akademie-Verlag, Berlin 1974.

[1.3] W. Schatt: Einführung in die Werkstoffkunde, VEB Deutscher Verlag für Grundstoffindustrie, Leipzig 1981.

[1.4] Järnets och stålets metallografi, Sandvikens Jernverks Aktibolag 1964.

[1.5] W. Schatt: Einführung in die Werkstoffkunde, VEB Deutscher Verlag für Grundstoffindustrie, Leipzig 1981.

[1.6] F. Wever and A. Rose.

[1.7] K. Honda and Z. Nihiyama.

[1.8] A.H.Cottrell: An introduction to Metallurgy, Edward Arnold (Publishers), London 1968.

[1.9] K.J. Irvine, Symposium: Steel-Strengthening Mechanisms, Zurich, May 5th and 6th 1969.

[1.10] I.J.Habraken and M.Economopoulos, Symposium: Transformation and Hardenability in Steels, Ann Arbor, Michigan, USA 1958.

[1.11] Sandvikens Jernverks Aktiebolag: Stål - struktur och värmebehandling, 1958.

[1.12] Atlas of Isothermal Transformation Diagrams, US Steel, Pittsburgh, 1951.

[1.13] Sandvikens Handbok, Del 7, Vol II, Sandvkens Jernverks Aktiebolag, 1964.

[1.14] Atlas of Isothermal Transformation Diagrams, US Steel, Pittsburgh, 1951.

[1.15] Atlas of Isothermal Transformation Diagrams, US Steel, Pittsburgh, 1951.

[1.16] Metals Handbook, Vol.4, 9.Edition, ASM, 1981.

[1.17] Metals Handbook, Vol.4, 9.Edition, ASM, 1981.

[1.18] E.C.Bain: Functions of the Alloying Elements in Steel, AMS, 1939.

[1.19] Sandvikens Handbok, Del 7, Vol II, Sandvikens Jernverks Aktiebolag, 1964.

[1.20] E.C.Bain: Functions of the Alloying Elements in Steel, AMS, 1939.

[1.21] K.J. Irvine, Symposium: Steel-Strengthening Mechanisms, Zurich, May 5th and 6th 1969.

[T.1.1] W. Schatt: Einführung in die Werkstoffwissenschaft. VEB Deutscher Verlag für Grundstoffindustrie, Leipzig 1981, S.55.